Minicourse on strongly correlated disordered systems

Eduardo Miranda

(Dated: May 10, 2025)

In this minicourse we will explore some aspects of the vast area of disordered strongly correlated materials. We plan to give a short exposition of the basic aspects of strongly correlated systems and some of the theoretical tools used to describe them. Among these we mention the Mott-Hubbard metal-insulator transition, large effective mass renormalization, local moment formation and the Kondo effect. We will give some emphasis to the theoretical advances that have been obtained through the Dynamical Mean Field Theory and its close descendants. The interplay of disorder and strong correlations leads to novel concepts that we will describe, such as disorder screening by interactions, Kondo disorder, electronic Griffiths phases, and others. We will show some of the experimental results that still defy our understanding and some initial steps that have been taken towards a complete description of these phenomena. Some of these ideas have been reviewed in E. Miranda and V. Dobrosavljević, "*Dynamical mean-field theories of correlation and disorder*," in *Conductor-Insulator Quantum Phase Transitions*, edited by V. Dobrosavljević, N. Trivedi, and J. M. Valles (Oxford University Press, 2012) p. 161.

CONTENTS

I. A STRONG CORRELATION PRIMER

The band theory of crystalline solid materials is very successful in describing electronic phenomena such as the distinction between metals, insulators and semiconductors. Small and simple adaptations can also explain various transport properties, shapes of Fermi surfaces, and impurity effects. Although this covers a lot of materials, there are still many more whose behavior requires a more detailed treatment of electron-electron interactions than is contained in most band theory calculations. These so-called strong correlation effects are central to the content of these lectures. A prominent example of these are the various types of magnetic order: ferromagnetism, antiferromagnetism, etc. These can only be explained if we take account of the electronic interactions. A simple way of seeing this is to realize that if you fill up the electronic bands according to the Pauli exclusion principle, gradually putting opposite spin pairs of electrons in each state of increasing energy, there will never be an imbalance of spin populations. We will see that Coulomb interactions are essential for that imbalance to occur.

A. The Hubbard model

The Hubbard model is the minimal model of a strongly correlated band. It is adequate as a simplified yet extremely rich description of the effects of Coulomb interactions on the behavior of electrons in bands derived from d-orbitals of transition metals. The most important effect is the Mott-Hubbard metal-insulator transition, a metal-insulator transition driven by electron-electron interactions. But it also covers other phenomena such as effective mass renormalizations, antiferromagnetism and, as many believe, high-temperature superconductivity.

The Hubbard model [1–4] Hamiltonian consists of two terms

$$H_{\text{Hub}} = -t \sum_{\langle i,j\rangle,\sigma} \left(c^{\dagger}_{i,\sigma} c_{j,\sigma} + \text{h.c.} \right) + U \sum c^{\dagger}_{i,\uparrow} c_{i,\uparrow} c^{\dagger}_{i,\downarrow} c_{i,\downarrow}, \tag{1}$$

where $c^{\dagger}_{i,\uparrow}\left(c_{i,\uparrow}\right)$ are spin-1/2 electron creation (annihilation) operators in the site basis. The first term describes hopping between sites and the second term describes the on-site Coulomb interaction between opposite spin electrons when they occupy the same site.

If $U = 0$ (the non-interacting limit), Fourier transforming to the $\mathbf{k}$ basis leads to

$$H^{\text{non-int}}_{\text{Hub}} = \sum_{\mathbf{k},\sigma} \epsilon_{\mathbf{k}} c^{\dagger}_{\mathbf{k},\sigma} c_{\mathbf{k},\sigma}, \tag{2}$$

where $c^{\dagger}_{\mathbf{k},\sigma}\left(c_{\mathbf{k},\sigma}\right)$ are creation (annihilation) operators in the $\mathbf{k}$ basis and

$$\epsilon_{\mathbf{k}} = -2t \left(\cos k_x + \cos k_y + \cos k_z\right), \tag{3}$$

is the band dispersion. The ground state corresponds to filling $\mathbf{k}$ states with up- and down-spin electrons up to the Fermi level so that we exhaust the total number of electrons N. Except in the limiting cases of $N = 0$ or $N = 2N_s$, where N_s is the total number of sites, we have an incompletely filled band. Low-lying excitations correspond to creating several particle-hole pairs. This is a simple metal, as a small electric field can easily make the electrons move, thus creating an electric current (a small resistance will always be present due to inevitable impurities and imperfections).

If, on the other hand, $t = 0$ (the atomic limit), the sites decouple from each other: states are localized on each site. Coulomb repulsion as expressed by the U-term penalizes double occupancy and a magnetic state in which a site has only one electron, either up or down is favored. Here we see how electronic repulsion favors magnetism.

When both t and U are different from zero, there is competition between delocalization, favored by t, and localization, favored by U. This is a very hard problem. If there is one electron per site, $N = N_s$, and $U \ll t$, delocalization wins and we have a half-filled band and a metal. If, on the other hand, $U \gg t$, electrons are localized, one per site, and they cannot move easily, e.g., by a small electric field, because any hop to a neighboring site would have to pay a large energy U: the system is a Mott insulator. This is not a band insulator. In band theory, a half-filled band is a metal. At some intermediate value of $U/t = (U/t)_c$, we expect a metal-Mott insulator transition. Some systems happen to naturally lie very close to $(U/t)_c$ and external or chemical pressure can tune the value of the ratio U/t (external pressure tends to increase t and has little effect on U, so pressure decreases U/t) and drive the system through a metal-Mott insulator transition.

B. The Heisenberg model

Consider now the Hubbard model at half-filling deep in the Mott insulating regime $U \gg t$. Electrons are localized, one at each site and there is no charge dynamics at energies much below U. But the electrons have spin and this situation says nothing about the spin dynamics. In fact, this is a massively spin-degenerate situation, since two spin configurations are possible on each site, and the low-energy manifold is 2^N-degenerate. We can ask ourselves what the spin dynamics is in a perturbation series in the small parameter t/U.

Using only words, the result of this analysis is the following. The first non-zero term is of second-order in t. Focus on two singly-occupied nearest-neighbor sites. If the electron spins are anti-aligned, the t-term can promote the hopping of one electron to the neighboring site, a state with energy U, and back, which is a process of $\mathcal{O}\left(t^2\right)$. This process can occur with or without a flip of the initial spins. As usual in second-order perturbation theory, this lowers the energy by a factor of $-t^2/U$. In contrast, if initially the electron spins are aligned, no such process can occur, because the hopping does not change the spin and two electrons of the same spin cannot doubly occupy a site. This is illustrated

in Fig. 1. Physically, second-order perturbation theory lowers the energy of anti-parallel spins and does nothing to parallel spins. This situation is described by the following Heisenberg Hamiltonian

$$H_{\rm Heis} = J \sum_{\langle i,j \rangle} \left(\mathbf{S}_i \cdot \mathbf{S}_j - \frac{1}{4} \right), \quad \left(J = \frac{4t^2}{U} \right). \tag{4}$$

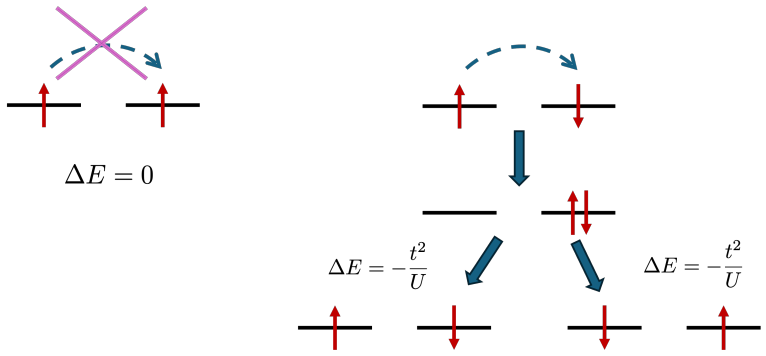

Figure 1. *Processes that contribute to super-exchange.* If initially the spins are parallel (left-hand side), virtual hopping is forbidden by the Pauli exclusion principle. If, on the other hand, the spins are initially anti-aligned, virtual hopping is allowed and the final configuration may have the initial spins flipped or not. Either way, there is a lowering of the energy by $-t^2/U$. The final effective Hamiltonian is the antiferromagnetic Heisenberg Hamiltonian of Eq. (4).

A few comments. J is indeed of order t^2/U, as anticipated (the factor of 4 comes from counting in how many ways the second order processes can occur). Clearly the positive value of J favors anti-alignment of neighboring spins. This is an antiferromagnetic coupling constant and this is an antiferromagnetic Heisenberg model. The Hamiltonian is invariant under a global rotation of all the spins. This is a consequence of the same symmetry that also exists in the Hubbard model. This type of interaction is called super-exchange [5]. It has this name because it occurs frequently in transition metal oxides, where an oxygen atom exists between the two transition metal atoms that experience this type of exchange and, despite their long separation, the antiferromagnetic coupling can be sizable.

Sure enough, of the many known Mott insulators, the great majority of them exhibit antiferromagnetic order at low enough temperatures.

C. The single-impurity Anderson model

An old problem in condensed matter physics was the following. Take a good metal, such as Cu, Ag or Au. Now grow some samples where you intermix a few percent magnetic ions, such as Fe or Co. These are ions with an incomplete $3d$-shell with a net spin and a magnetic moment (focus only on the spin magnetic moment). It is not clear that the magnetic moment will survive in the alloy. For one thing, the $3d$-state can quantum-mechanically mix (hybridize) with the itinerant metallic states of the matrix and get "dissolved" in the conduction band, forming non-magnetic impurity states. On the other hand, if the hybridization is not strong enough, the state may remain localized in the $3d$-shell and retain its magnetic character. The question is: What determines what actually happens?

This state of affairs was studied for the first time by P. W. Anderson [6], who proposed the following bare-bones model Hamiltonian to describe this situation

$$H_{\rm And} = \sum_{\mathbf{k},\sigma} \epsilon_{\mathbf{k}} c^\dagger_{\mathbf{k},\sigma} c_{\mathbf{k},\sigma} + \sum_{\sigma} \epsilon_d d^\dagger_\sigma d_\sigma + \sum_{\mathbf{k},\sigma} V \left(c^\dagger_{\mathbf{k},\sigma} d_\sigma + d^\dagger_\sigma c_{\mathbf{k},\sigma} \right) + U d^\dagger_\uparrow d_\uparrow d^\dagger_\downarrow d_\downarrow. \tag{5}$$

Here, $d^\dagger_\sigma$ (d_σ) creates (annihilates) spin-1/2 electron on the $3d$-impurity site (whose energy is ϵ_d), while $c^\dagger_{\mathbf{k},\sigma}$ $\left(c_{\mathbf{k},\sigma}\right)$ creates (annihilates) spin-1/2 electrons in the conduction band $\mathbf{k}$-state (whose energy is $\epsilon_{\mathbf{k}}$). The strength of hybridization between the impurity state and the band is given V, as described by the third term. The last term, responsible for the appearance of the magnetic configuration, is a Hubbard-like interaction term. It is the competition between V, which favors dissolving the state into the band, and the U-term, which favors magnetism, that lies at the heart of the problem.

If $U = 0$, we have non-interacting impurity hybridizing with the conduction band. The localized impurity state with energy ϵ_d mixes with the conduction band states with similar energies $\epsilon_{\mathbf{k}} \approx \epsilon_d$ and turns into a Lorentzian "resonance" of width $\Gamma = \pi\rho(\epsilon_d)V^2$, where $\rho(\epsilon_d)$ is the conduction band density of states at energy ϵ_d. The impurity density of states is

$$\rho_d(\omega) = \frac{1}{\pi}\frac{\Gamma}{(\omega - \epsilon_d)^2 + \Gamma^2}. \tag{6}$$

This is a non-magnetic situation, because, as usual, the resonance gets filled with equal spin-up and spin-down population: $\langle n_{d\uparrow}\rangle = \langle n_{d\downarrow}\rangle$.

If, on the other hand, $V = 0$,the impurity state decouples from the band and, if

$$\epsilon_d < 0 \text{ and } \epsilon_d + U > 0, \tag{7}$$

the lowest-energy configuration has single occupancy of the d-orbital with either $n_{d\uparrow} = 1$ or $n_{d\downarrow} = 1$: a magnetic state.

If now we turn on both U and V, the situation is much more complex. However, using a mean-field analysis, Anderson showed that there is still a region of parameter space in which the magnetic state survives. Fig. 2 below shows the region of stability of local moments in the $V = 0$ case (blue region) and when $V \neq 0$ (orange region). Turning on V clearly shrinks the region of local moment stability, but it still survives for large enough U.

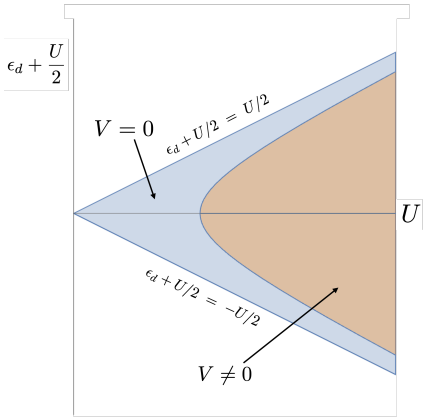

Figure 2. In the $\epsilon_d + U/2$ vs U parameter space, the regions of stability of local moments are shown in the $V = 0$ case (blue region) and when $V \neq 0$ (orange region).

The magnetic states found by Anderson correspond to two degenerate ground states in which either $\langle n_{d\uparrow}\rangle \approx 1$ and $\langle n_{d\downarrow}\rangle \approx 0$ or $\langle n_{d\uparrow}\rangle \approx 0$ and $\langle n_{d\downarrow}\rangle \approx 1$. Each of them is a spontaneously broken (time-reversal) symmetry state. However, general theorems forbid broken symmetries at any temperature in systems with only a few degrees of freedom (in this case, essentially one orbital). So, although these magnetic states are physically meaningful at intermediate temperatures, with corresponding Curie-like magnetic susceptibilities

$$\chi_{\text{Curie}}(T) = \frac{g^2\mu_B^2}{4k_BT}, \tag{8}$$

they cannot survive at lower temperatures. Fluctuations going beyond mean field will restore the broken symmetry. What model describes this symmetry-restoring process?

D. The Kondo model

As we saw in the case of the half-filled Hubbard model at strong coupling $U \gg t$, the charge is frozen and the low-energy spin dynamics is effectively governed by the Heisenberg model. Analogously, we can use second-order perturbation theory to describe the spin-flip dynamics that take the magnetic state with $\langle n_{d\uparrow}\rangle \approx 1$ and $\langle n_{d\downarrow}\rangle \approx 0$ to magnetic state with $\langle n_{d\uparrow}\rangle \approx 0$ and $\langle n_{d\downarrow}\rangle \approx 1$. Obviously, it is the conduction electrons that are responsible for the spin processes. Indeed, this is described by the Kondo Hamiltonian

$$H_{\text{Kondo}} = \sum_{\mathbf{k},\sigma}\epsilon_{\mathbf{k}}c^\dagger_{\mathbf{k},\sigma}c_{\mathbf{k},\sigma} + \sum_{\mathbf{k},\mathbf{q},\alpha,\beta} J_K\left(c^\dagger_{\mathbf{k},\alpha}\boldsymbol{\sigma}_{\alpha\beta}c_{\mathbf{k},\beta}\right)\cdot\mathbf{S}, \tag{9}$$

where $\boldsymbol{\sigma} = (\sigma_x, \sigma_y, \sigma_z)$ are the Pauli matrices, $\mathbf{S} = (S_x, S_y, S_z)$ are spin-1/2 operators describing the spin of the singly-occupied $3d$ orbital, and

$$J_K \approx 2V^2 \left(\frac{1}{\epsilon_d + U} - \frac{1}{\epsilon_d} \right) > 0, \tag{10}$$

is the Kondo exchange coupling constant. Note that, because the conditions (7) for the magnetic state apply, this is an antiferromagnetic coupling. Fig. 3 illustrates the second-order virtual processes that lead to the Kondo Hamiltonian.

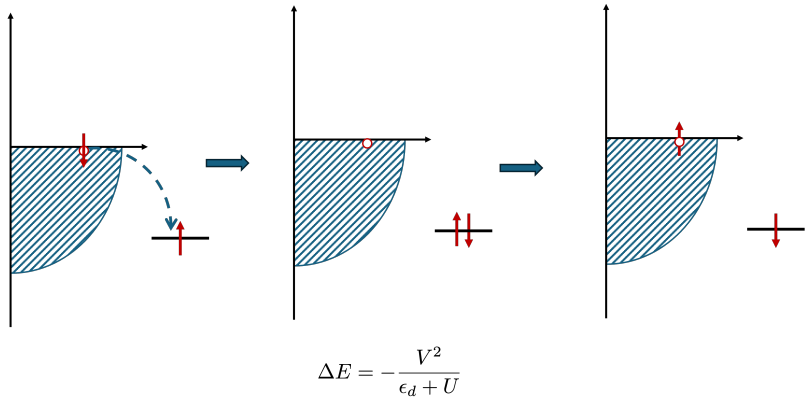

Figure 3. In the regime of local moment stability, virtual processes of order $\mathcal{O}\left(V^2\right)$ involving the localized electron and conduction electrons at the Fermi level lead to Kondo Hamiltonian of Eq. (9) with coupling constant given by Eq. (10).

The low-temperature fate of the local moment is a complex highly-entangled many-body state in which the localized spin forms a singlet state with effectively one conduction electron which is, however, spread out in a "Kondo cloud" around the impurity. The gradual process of this Kondo singlet formation as the temperature is lowered took many years to elucidate [7–13]. However, it is now well understood. The magnetic susceptibility of the Kondo model is shown in Fig. 4(a). The A curve shows clearly a stable local moment at intermediate temperatures and the "quenching" of the local moment at lower temperatures.

The Kondo model has a unique characteristic energy scale that separates high temperatures from low temperatures. That is the Kondo temperature, whose expression is

$$T_K = D \exp\left(-\frac{1}{\rho_F J_K} \right), \tag{11}$$

where D and ρ_F are the conduction band half-width and density of states at the Fermi level. Every dimensionless property of the model can be written as a *universal scaling function* of temperature T, frequency ω and magnetic field B, all scaled appropriately by T_K, of the form (if the quantity is not dimensionless, dimensionful pre-factors multiply the scaling functions)

$$F\left(\frac{T}{T_K}, \frac{\omega}{k_B T_K/\hbar}, \frac{B}{k_B T_K/g\mu_B} \right). \tag{12}$$

As an example of this kind of scaling behavior, the susceptibility of the Kondo model is shown in Fig. 4(b).

E. A mathematical description of the Anderson/Kondo single-impurity model

For later reference, we will discuss now some important features of the Anderson single-impurity model of Eq. (5). A great deal of insight into the physics of the model is obtained by analyzing the d-level Green function. This is defined by the following expression (this is the so-called retarded Green function)

$$G_d\left(t - t'\right) = -i\theta\left(t - t'\right) \left\langle \left\{ d_\sigma\left(t\right), d_\sigma^\dagger\left(t'\right) \right\} \right\rangle, \tag{13}$$

where the expectation value is an equilibrium ensemble average

$$\langle O \rangle = \frac{\mathrm{Tr}\left[e^{-\beta H_{\mathrm{And}}} O \right]}{Z}, \tag{14}$$

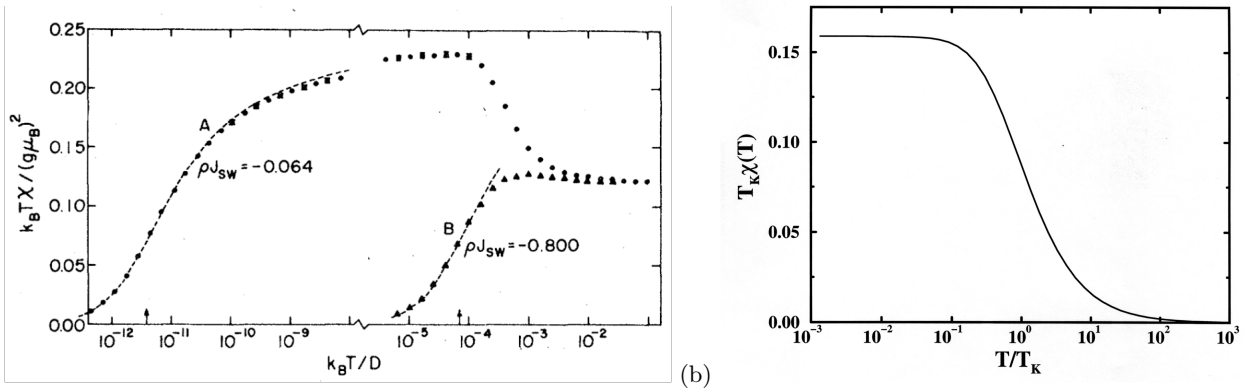

Figure 4. (a) Magnetic susceptibility of the Anderson model. Curve A: there is a wide temperature range where the local moment is well developed ($T\chi(T) \sim 1/4$); at lower temperatures, $T \ll T_K$, $\chi(T) \sim$ const.. Curve B: there is never a regime with a well-developed local moment. The Kondo temperatures are shown as vertical arrows on the horizontal axis. From ref. [14]; (b) Magnetic susceptibility of the Kondo model showing scaling behavior with T_K.

$\theta(t)$ is the Heaviside step function

$$\theta(t) = \begin{cases} 1 & \text{if } t > 0, \\ 0 & \text{if } t < 0, \end{cases}$$

and the time dependence of operators is provided by the Heisenberg picture

$$O(t) = e^{-iH_{\text{And}}t} O e^{iH_{\text{And}}t}. \tag{15}$$

This rather strange-looking object provides a great deal of information on the local d-electron dynamics. Its Fourier transform is very illuminating

$$G_d(\omega) = \int_{-\infty}^{\infty} G_d(T)\, e^{i(\omega+i\eta)T} dT = \frac{1}{\omega - \epsilon_d - \Delta(\omega) - \Sigma(\omega)}, \tag{16}$$

where $T = t - t'$ (it can be shown that the Green function of Eq. (13) depends only on the difference $t - t'$),

$$\Delta(\omega) = \sum_{\mathbf{k}} \frac{V^2}{\omega + i\eta - \epsilon_{\mathbf{k}}} = \int \rho(\epsilon) \frac{V^2}{\omega + i\eta - \epsilon} d\epsilon, \tag{17}$$

is the so-called hybridization function, $\rho(\epsilon)$ is the density of states of the conduction band, and $\Sigma(\omega)$ is the self-energy. The infinitesimal imaginary term $i\eta$ is introduced to ensure the convergence of the Fourier transform. The hybridization function describes the probability for the electron to hop on and off the impurity site, whereas $\Sigma(\omega)$ encapsulates all the effects of interactions. If $U = 0$, then $\Sigma(\omega) = 0$. Of course, it is difficult to obtain $\Sigma(\omega)$, but I can tell you that there are several reliable tools that can be used to calculate it, each with their own pros and cons.

Let me describe a few known facts about $G_d(\omega)$ and $\Sigma(\omega)$. The imaginary part of $G_d(\omega)$ gives the spectral function of the d-level, informally called the local density of states projected of the d-level

$$\rho_d(\omega) = -\frac{1}{\pi}\text{Im}\left[G_d(\omega)\right] = \frac{1}{\pi} \frac{\text{Im}\left[\Delta(\omega) + \Sigma(\omega)\right]}{\left\{\omega - \epsilon_d - \text{Re}\left[\Delta(\omega) + \Sigma(\omega)\right]\right\}^2 + \left\{\text{Im}\left[\Delta(\omega) + \Sigma(\omega)\right]^2\right\}}. \tag{18}$$

This quantity measures the response of the system when you create or destroy an electron in the d-orbital, e.g., by impinging the system with light. Thus, it can be measured in experiments like photoemission spectroscopy (in the photoelectric effect). Fig. 5 shows this quantity for different values of U and $\omega > 0$ for a model with $\epsilon_d = -U/2$ (the so-called particle-hole symmetric case) [15]. This function is an even function of ω, so the behavior for negative ω is the mirror reflection with respect to the vertical axis. The generic structure of this quantity is a narrow peak centered at $\omega = 0$ (the Fermi level) and two broad peaks at around $\omega \approx \pm U/2$. The broad peak locations correspond to the energy differences for transitions from the ground state, with a singly-occupied state, to the empty or to the doubly-occupied level, as follows

$$\begin{aligned} n_d = 1 \to n_d = 0 \;&\Rightarrow\; \Delta E = \epsilon_d = -U/2, \\ n_d = 1 \to n_d = 2 \;&\Rightarrow\; \Delta E = \epsilon_d + U = U/2. \end{aligned}$$

The narrow peak at $\omega = 0$, on the other hand, is related to very low-energy transitions between states close to the Fermi level, and involve no real change of occupation $n_d = 1$. These are spin-fluctuation processes well described by the effective Kondo Hamiltonian of Eq. (9), which is why this peak is known as the Kondo resonance or the Kondo peak. The width of this peak is of the order of the Kondo temperature

$$T_K = D \exp\left(-\frac{U}{8\rho_F V^2}\right) = D \exp\left(-\frac{\pi U}{8\mathrm{Im}\left[\Delta\left(0\right)\right]}\right), \tag{19}$$

which is obtained using Eqs. (11) and (10). Note how this energy scale decreases rapidly with increasing U.

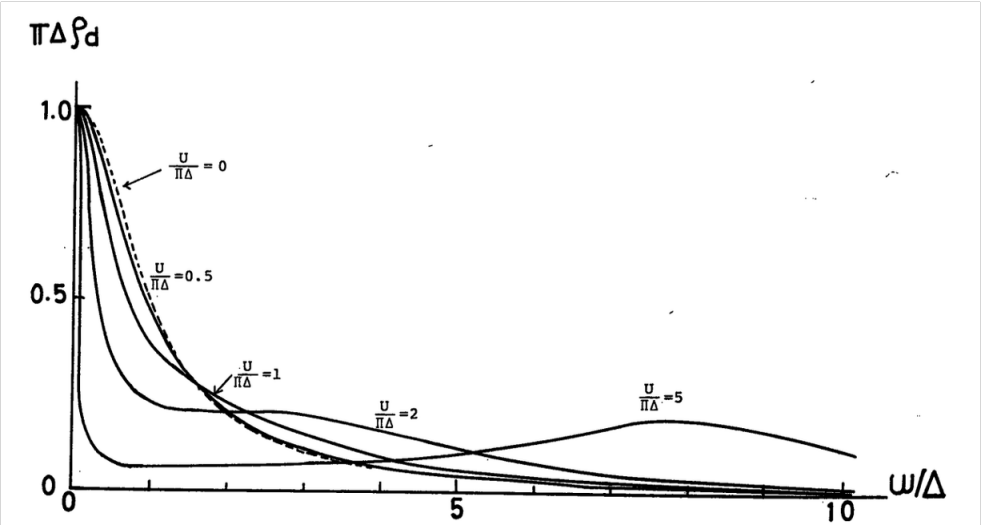

Figure 5. Spectral function (also called the local density of states) for the symmetric single-impurity Anderson model, see Eq. (18), for various values of interaction U. From ref. [15].

The spectral function $\rho_d\left(\omega\right)$ can be measured in experiments of photoemission spectroscopy (PES) for $\omega < 0$ and inverse photoemission spectroscopy (also called Bremsstrahlung Isochromat Spectroscopy or BIS) for $\omega > 0$. Fig. 6(a) shows the combined PES and BIS spectra for some systems in which a Ce^{3+} ion exhibits a local moment with one electron in the f-shell, $n_f = 1$, and the Kondo effect. The spectra can be analyzed as giving $\rho_d\left(\omega\right)$ for the Ce ion. In both cases, broad peaks away from the Fermi energy ($\omega = 0$) can be seen, corresponding to the $n_f = 1 \to n_f = 0$ (in the $\omega < 0$ region) and the $n_f = 1 \to n_f = 2$ (in the $\omega > 0$ region) transitions. In the case of CeAl, the Kondo temperature is too small and no peak can be discerned at the Fermi energy within the experimental resolution. For $CeNi_2$, however, a clear Kondo peak is visible close to $\omega = 0$. Fig. 6(b) shows results of PES for different Ce-based materials, with different values of the Kondo temperature: the larger T_K, the broader the Kondo peak.

1. *The low-energy Fermi liquid regime*

Further insight into this behavior can be gleaned from a low-energy, low-temperature description of the self-energy $\Sigma\left(\omega\right)$ that goes under the name of Fermi liquid theory. The original Fermi liquid theory was proposed by Landau to describe the low-temperature behavior of fermionic systems such as the helium isotope ^{3}He [18–20]. But it was later generalized to describe the low-energy, low-temperature behavior of the Anderson/Kondo single-impurity model [21, 22]. The low-energy behavior of $\Sigma\left(\omega\right)$ is parametrized by

$$\Sigma\left(\omega\right) \approx \delta - a\omega - i\Gamma, \tag{20}$$

with

$$\Gamma \approx \begin{cases} b\omega^2 & \text{if } \omega > T \\ b'T^2 & \text{if } \omega < T \end{cases}, \tag{21}$$

where the constants $\delta, a, b, b' \in \mathbb{R}$ and a, b, b' are all positive . First note that, to leading linear order in ω and T, $\Sigma\left(\omega\right) \in \mathbb{R}$. To see how this affects the local Green function, take the following low-energy limit of the hybridization

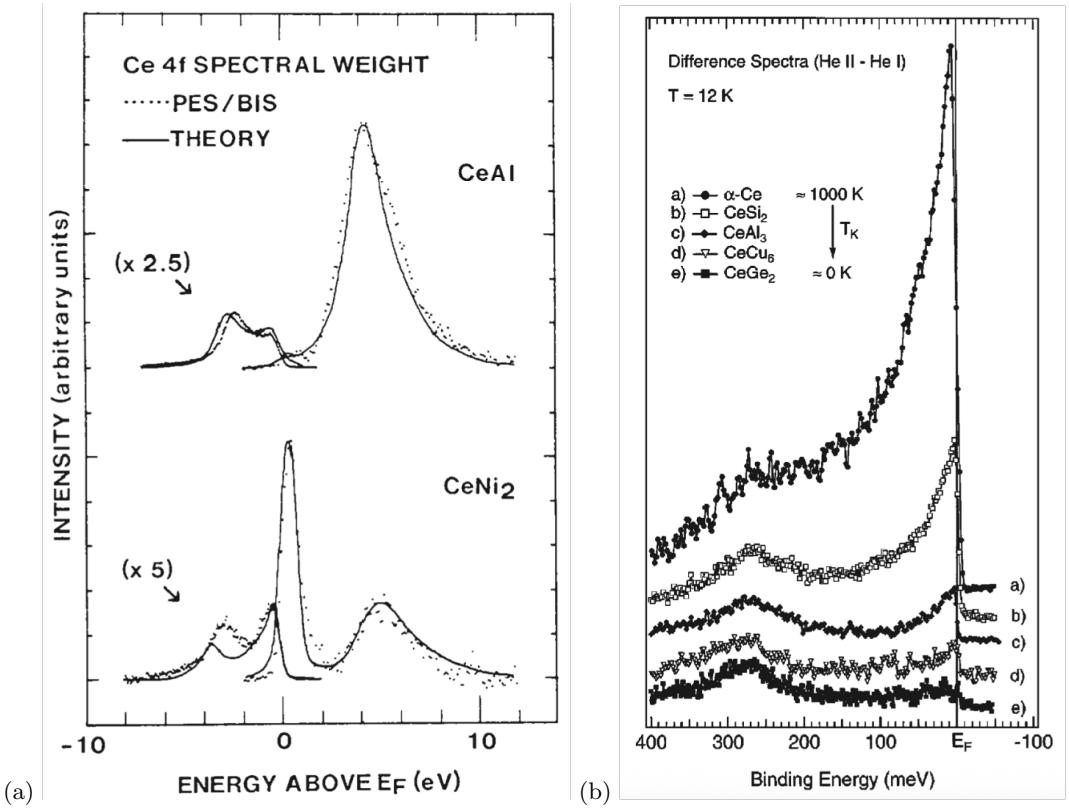

Figure 6. (a) Combined photoemission (PES) and BIS spectra for two different Ce-based local moment systems, showing the generic features of the spectral function of the Anderson single-impurity model. In the case of CeAl, the Kondo temperature is too small for the Kondo peak to be discerned. From ref. [16]; (b) PES results for Ce-based compounds with different values of the Kondo temperature with correspondingly different Kondo resonance widths. From ref. [17].

function of Eq. (17) (the infinitesimal $i\eta$ is necessary)

$$\Delta(\omega) = \sum_{\mathbf{k}} \frac{V^2}{\omega + i\eta - \epsilon_{\mathbf{k}}} \approx \Delta'(0) - i\Delta''(0). \tag{22}$$

In the non-interacting limit, $\Sigma(\omega) = 0$ and plugging Eq. (22) into Eq. (18) gives us

$$\rho_d^{\text{non-int}}(\omega) = \frac{\Delta''(0)/\pi}{\{\omega - \epsilon_d - \Delta'(0)\}^2 + [\Delta''(0)]^2}, \tag{23}$$

which is a Lorentzian centered at $\Delta'(0)$ of width $\Delta''(0)$.

Using now the Fermi liquid self-energy of Eq. (20) we get

$$G_d(\omega) = \frac{1}{(1+a)\,\omega - \epsilon_d - \Delta'(0) - \delta + i\,[\Delta''(0) + \Gamma]} \tag{24}$$

$$= \frac{Z}{\omega - Z\epsilon_d - Z\Delta'(0) - Z\delta + iZ\Delta''(0)} \tag{25}$$

$$= \frac{Z}{\omega - \tilde{\epsilon}_d - \tilde{\Delta}'(0) - \tilde{\delta} + i\left[\tilde{\Delta}''(0) + \tilde{\Gamma}\right]}, \tag{26}$$

where we defined the quasi-particle weight (or wave function renormalization)

$$Z = \frac{1}{1+a} \in (0, 1], \tag{27}$$

and a tilde over a symbol means it has been multiplied by Z, $\tilde{\delta} = Z\delta$, etc. We refer to the quantities adorned by a tilde as renormalized quantities. The local density of states is obtained from the imaginary part of the d-level Green

function, see Eq. (18),

$$\rho_d(\omega) = \frac{1}{\pi} \frac{Z\left[\tilde{\Delta}''(0) + \tilde{\Gamma}\right]}{\left[\omega - \tilde{\epsilon}_d - \tilde{\Delta}'(0) - \tilde{\delta}\right]^2 + \left[\tilde{\Delta}''(0) + \tilde{\Gamma}\right]^2}. \tag{28}$$

Fermi liquid theory also dictates that for the Kondo resonance

$$\tilde{\epsilon}_d + \tilde{\Delta}'(0) + \tilde{\delta} \approx 0, \tag{29}$$

so that the renormalized resonance is centered at the Fermi level. This reflects the physics that the Kondo effect involves electrons at the Fermi energy, so that the Kondo resonance is inextricably tied to the Fermi level. We call this Fermi level pinning of the Kondo resonance.

Besides, the resonance width is

$$\tilde{\Delta}''(0) + \tilde{\Gamma}, \tag{30}$$

which reduces at zero temperature to [see Eq. (19)]

$$\tilde{\Delta}''(0) = T_K. \tag{31}$$

The width increases as the temperature is raised, because of the increase of $\tilde{\Gamma}$ with temperature. Note that

$$Z = \frac{\tilde{\Delta}''(0)}{\Delta''(0)} = \frac{T_K}{\Delta''(0)}. \tag{32}$$

Inspection of Fig. 5 as well as Eq. (19) both show that the zero-temperature resonance width decreases rapidly with the increase of the interaction U, and so does Z. Thus, the quasi-particle weight becomes very small for large U, although it never vanishes.

Finally, the peak height at $T = 0$ is

$$\rho_d(0) = \frac{1}{\pi} \frac{Z}{\tilde{\Delta}''(0)} = \frac{1}{\pi} \frac{1}{\Delta''(0)}, \tag{33}$$

which is, surprisingly, not renormalized by interactions, compare it with Eq. (23). This is also consistent with the behavior seen in Fig. 28. Finally, integrating Eq. (28)

$$\int_{-\infty}^{\infty} d\omega \rho_d(\omega) = Z, \tag{34}$$

and the *spectral weight of the Kondo resonance* is given by the quasi-particle weight Z.

Let us now highlight the main features of the Kondo resonance:

1. The Kondo resonance is pinned to the Fermi level, see Eq. (29).
2. The width of the Kondo resonance is T_K at $T = 0$ but increases as the temperature is raised, see Eqs. (30) and Eq. (31). At $T = 0$, it decreases rapidly with increasing U, see Eq. (19).
3. The height of the Kondo resonance is unaffected by interactions, see Eq. (33).
4. The quasi-particle weight Z causes the renormalization of the Kondo resonance width and the imaginary part of the self-energy and it also gives the spectral weight of the Kondo resonance, see Eq. (34). At $T = 0$, it is a rapidly decreasing function of the interaction U, see Eqs. (19) and (32).

All of these facts will be important for the subsequent analysis.

II. THE DYNAMICAL MEAN-FIELD THEORY (DMFT)

An exact treatment of a generic interacting lattice Hamiltonian can only be achieved numerically, with well-known limitations. Irrespective of this, a qualitative understanding of the physics is what is desired. In this case, approximate

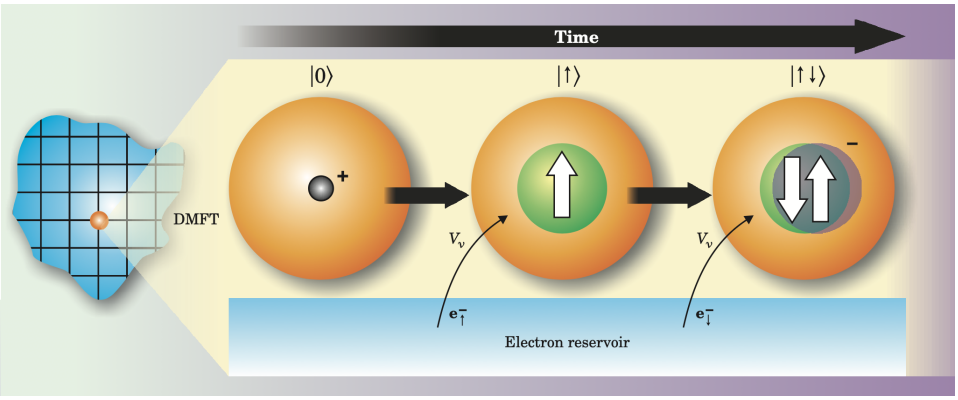

Figure 7. In the DMFT, we focus on the dynamics of a single lattice site. We simplify its dynamics by assuming the only effect of the rest of the lattice is to exchange electrons with that site. As time goes by, the occupancy of the site fluctuates from empty, $|0\rangle$, to singly-occupied, $|\uparrow\rangle$ or $|\downarrow\rangle$, to doubly-occupied, $|\uparrow\downarrow\rangle$, and so on. The rest of the lattice acts as an electron reservoir. Figure taken from ref. [24].

treatments are inevitable. Prominent among these is the Dynamical Mean Field Theory (DMFT) [23]. We will give a brief outline of how it works. We will use the Hubbard model as example.

The DMFT approach starts by focusing on the dynamics of a single site of the lattice, say the site at the origin $\mathbf{R} = 0$. That site can be seen as an "impurity" embedded in the rest of the lattice. The dynamics of this impurity in contact with the rest of the lattice is extremely complicated. However, we can take a simplified approach to its dynamics and consider that the *only effect of the rest of the lattice is to exchange electrons with the impurity.* As time goes by, electrons can hop on the impurity from the lattice and off the impurity back into the lattice (see Fig. 7). The rest of the lattice acts as an electron reservoir.

From the point of view of the site at the origin, it is just like the d-level of the Anderson single-impurity Hamiltonian of Eq. (5) with $\epsilon_d = 0$. The question is: what should we take as the conduction electron band? Well, we can think of it as the rest of the lattice minus the site at the origin. But we must find the correct band dispersion $\epsilon_{\mathbf{k}}$ and hybridization V that mimic the effect of the rest of the lattice on the site at the origin.

The physics of the single electron hopping on and off the interacting site of Eq. (5) is captured by its Green function $G_d(\omega)$, defined previously in Eqs. (13) and (16). As stated before, the difficult task is to obtain the self-energy $\Sigma(\omega)$. There are many methods of determining the self-energy, analytically or numerically, with different levels of accuracy. These methods are called "impurity solvers". There is a vast literature on these solvers but I will not go into their detail. I will assume that $\Sigma(\omega)$ can be found somehow. Note, crucially, that $\Sigma(\omega)$ is an implicit functional of $\Delta(\omega)$ and U, in other words, given $\Delta(\omega)$ and U we can uniquely find $\Sigma(\omega)$. This situation can be usefully highlighted by making the dependence explicit

$$\Sigma(\omega) \equiv \Sigma[\Delta(\omega), U, \omega]. \tag{35}$$

But this is just the dynamics of the impurity site for given $\Delta(\omega)$ and U. What about the rest of the lattice? Well, one can also define the lattice Green function. Since it has lattice translation invariance, we can define it in $\mathbf{k}$-space as

$$G_{\text{latt}}(\mathbf{k}, t-t') = -i\theta(t-t')\left\langle \left\{ c_{\mathbf{k}\sigma}(t), c^\dagger_{\mathbf{k}\sigma}(t') \right\} \right\rangle, \tag{36}$$

and its Fourier transform can also be parametrized by a lattice self-energy $\Sigma_{\text{lat}}(\mathbf{k}, \omega)$ as

$$G_{\text{lat}}(\mathbf{k}, \omega) = \frac{1}{\omega - \epsilon_{\mathbf{k}} - \Sigma_{\text{lat}}(\mathbf{k}, \omega)}. \tag{37}$$

Again, if $U = 0$, then $\Sigma_{\text{lat}}(\mathbf{k}, \omega) = 0$. Now, the DMFT "recipe" starts by

(1) assuming that the lattice self-energy is k-independent,

$$\Sigma_{\text{lat}}(\mathbf{k}, \omega) \to \Sigma^{\text{DMFT}}_{\text{lat}}(\omega). \tag{38}$$

Note that $\mathbf{k}$-independence implies a *local* self-energy, in the sense that its space-dependent counterpart is *site-diagonal and site-independent*

$$\Sigma_{\text{lat}}(\mathbf{R}_i - \mathbf{R}_j, \omega) = \sum_{\mathbf{k}} e^{-i\mathbf{k}\cdot(\mathbf{R}_i - \mathbf{R}_j)} \Sigma_{\text{lat}}(\mathbf{k}, \omega)$$

$$\rightarrow \sum_{\mathbf{k}} e^{-i\mathbf{k}\cdot(\mathbf{R}_i-\mathbf{R}_j)}\Sigma_{\text{lat}}^{\text{DMFT}}(\omega) = \delta_{\mathbf{R}_i,\mathbf{R}_j}\Sigma_{\text{lat}}^{\text{DMFT}}(\omega). \tag{39}$$

So, in DMFT,

$$G_{\text{lat}}(\mathbf{k},\omega) = \frac{1}{\omega - \epsilon_{\mathbf{k}} - \Sigma_{\text{lat}}^{\text{DMFT}}(\omega)}. \tag{40}$$

Furthermore, DMFT also makes the following reasonable self-consistency assumptions:

(2) the local self-energy of the lattice must be the same as the self-energy of the impurity problem

$$\Sigma_{\text{lat}}^{\text{DMFT}}(\omega) = \Sigma(\omega), \tag{41}$$

and

(3) the local part of the lattice Green function must coincide with the Green function of the "impurity" site of Eq. (16).

The local part of the lattice Green function is obtained from doing first the inverse Fourier transform to real space

$$G_{\text{lat}}(\mathbf{R}_i - \mathbf{R}_j, \omega) = \sum_{\mathbf{k}} e^{-i\mathbf{k}\cdot(\mathbf{R}_i-\mathbf{R}_j)} G_{\text{lat}}(\mathbf{k},\omega),$$

and then making $\mathbf{R}_i = \mathbf{R}_j$ to extract the local part

$$G_{\text{lat}}(\mathbf{0},\omega) = \sum_{\mathbf{k}} G_{\text{lat}}(\mathbf{k},\omega) = \sum_{\mathbf{k}} \frac{1}{\omega - \epsilon_{\mathbf{k}} - \Sigma_{\text{lat}}^{\text{DMFT}}(\omega)}, \tag{42}$$

and finally equating this to Eq. (16) and imposing $\Sigma_{\text{lat}}^{\text{DMFT}}(\omega) = \Sigma(\omega)$,

$$\sum_{\mathbf{k}} \frac{1}{\omega - \epsilon_{\mathbf{k}} - \Sigma[\Delta(\omega), U, \omega]} = \frac{1}{\omega - \Delta(\omega) - \Sigma[\Delta(\omega), U, \omega]}, \tag{43}$$

where we made again explicit that the self-energy is defined by both U and $\Delta(\omega)$, see Eq. (35). It is clear that the Hubbard model is defined by giving $\epsilon_{\mathbf{k}}$ and U. The impurity self-energy is a functional of the hybridization and U. Therefore, the self-consistency condition of Eq. (43) is an implicit equation for the hybridization $\Delta(\omega)$. This defines the solution to the problem uniquely.

We have described the DMFT recipe by (1) assuming the effects of correlations are local (Eq. (38)) and by (2) appealing to physical arguments to arrive at the self-consistency condition (Eq. (43)). Historically, however, DMFT was first deduced as the exact theory of the Hubbard model in infinite dimensions [25]. It is nice to have a well-defined limit in which the approach is exact. Nonetheless, it is perhaps better to think of DMFT as an approximate theory of finite-dimensional systems that provides the optimal description that *incorporates only local effects of correlations*. The approach expounded above, which views DMFT as *an impurity problem plus a self-consistency condition* is the one that is most physically fruitful, since we have a very good knowledge of the physics of the single-impurity Anderson model. This approach was developed after the infinite-dimensional viewpoint [26].

Summing up, the algorithm for solving the Hubbard model within DMFT is:

1. Start with an initial guess for the hybridization function $\Delta(\omega)$.
2. Solve the impurity problem using some impurity solver to find $G_d(t-t') = -i\theta(t-t')\left\langle\left\{d_\sigma(t), d_\sigma^\dagger(t')\right\}\right\rangle$.
3. Obtain its Fourier transform $G_d(\omega)$.
4. Find the self-energy from $\Sigma(\omega) = \omega - \Delta(\omega) - [G_d(\omega)]^{-1}$ [Eq. (16)].
5. Use the self-energy to get the local lattice Green function

$$G_{\text{lat}}(\mathbf{0},\omega) = \sum_{\mathbf{k}} \frac{1}{\omega - \epsilon_{\mathbf{k}} - \Sigma(\omega)}. \tag{44}$$

6. Obtain a new hybridization function from [Eq. (43)]

$$\Delta_{\text{new}}(\omega) = \omega - \Sigma(\omega) - [G_{\text{lat}}(\mathbf{0},\omega)]^{-1}. \tag{45}$$

7. Test if $\Delta_{\text{new}}(\omega) = \Delta(\omega)$. If yes, self-consistency has been reached. If not, use $\Delta_{\text{new}}(\omega)$ as the new hybridization function and go back to step 1.

A. The Mott transition according to DMFT

One of the earliest successes of the DMFT was the description of the Mott-Hubbard metal-insulator transition [27–29] of the half-filled Hubbard model. This is best illustrated by the local spectral function (loosely called the density of states), given by the imaginary part of the local Green function

$$\rho_d(\omega) = \mathrm{Im}\left[G_d(\omega)\right] = \mathrm{Im}\left[\frac{1}{\omega - \Delta(\omega) - \Sigma(\omega)}\right]. \tag{46}$$

Fig. 8(a) shows $\rho_d(\omega)$ as U increases from top to bottom. At small U, density of states is that of a half-filled metallic band. As U increases, three features can be discerned. A narrow central quasiparticle peak, corresponding to long-lived itinerant metallic carriers, and two broad higher-energy bands, called lower and upper Hubbard bands. The latter correspond to incoherent excitations that are short-lived. At the highest U value, the quasiparticle peak has disappeared and there is a well-formed gap between lower and upper Hubbard bands. This is the Mott-Hubbard insulator. We note that, in terms of the dynamics of the local site, the lower and upper Hubbard bands correspond to the local moment formation of Anderson's mean-field theory of the single-impurity model. The quasiparticle peak, on the other hand, is connected to the low-energy Kondo fluctuations (the Kondo resonance). The Kondo resonance and the lower Hubbard band can be seen in PES experiments and compared to the DMFT predictions. This was performed in ref. Mo *et al.* [30] where realistic band strucutre of V_2O_3 was combined with DMFT in order to obtain the PES curve, as seen in Fig. 8(b). The agreement is reasonably good.

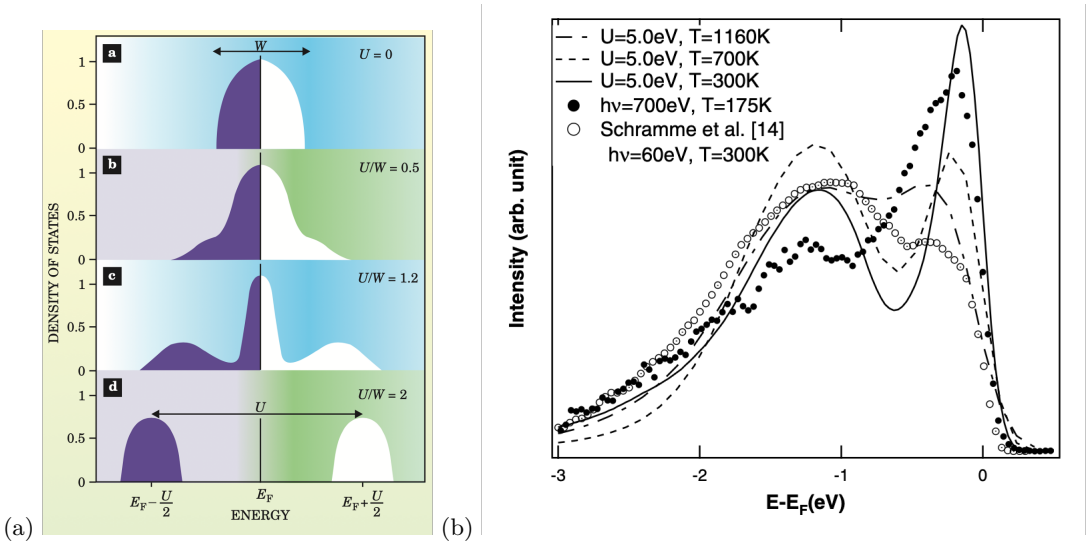

Figure 8. (a) The local density of states of the half-filled Hubbard model as given by DMFT. W here is the band width. Figure taken from ref. [24]. (b) Photoemission spectroscopy measurements for V_2O_3 compared with DMFT + band structure calculations. Figure taken from ref. [30].

DMFT also gives a non-trivial T vs. U phase diagram, as seen in Fig. 9. The dashed line is the Mott-Hubbard phase transition line $U_c(T)$. The treatment indicates that this is a first-order phase transition, featuring a discontinuous jump from a metal (Fermi liquid) to a paramagnetic insulator (say, from Fig. 8(c) to Fig. 8(d)). As in other first-order transitions, there is a region of "coexistence" between the two phases (yellow region around the transition line). Within this region, there can be a metastable insulating phase if $U_{c1}(T) < U < U_c(T)$, where $U_{c1}(T)$ is the continuous line bounding the yellow region on its left-hand side. Likewise, a metastable metallic phase exists if $U_c(T) < U < U_{c2}(T)$, where $U_{c2}(T)$ is the continuous line bounding the yellow region on its right-hand side. We stress that these are not the thermodynamically stable phases. There is a close analogy to the superheating and supercooling of liquids. Outside the coexistence region, however, only the thermodynamically stable phase is possible. The continuous lines that define the coexistence region, $U_{c1}(T)$ and $U_{c2}(T)$, are called spinodal lines.

The first-order line terminates at a second-order critical point where the transition is continuous and the quasiparticle peak width shrinks smoothly to zero. This is also very reminiscent of the liquid-gas transition line, which is also first-order terminating at a second-order critical point. As in the liquid-gas case, one can go continuously "around" the critical point from the metal to insulator without ever crossing the phase transition line. Just like in the liquid-gas case, there is no sharp distinction between a metal and an insulator at finite temperatures, as the resistivity is always

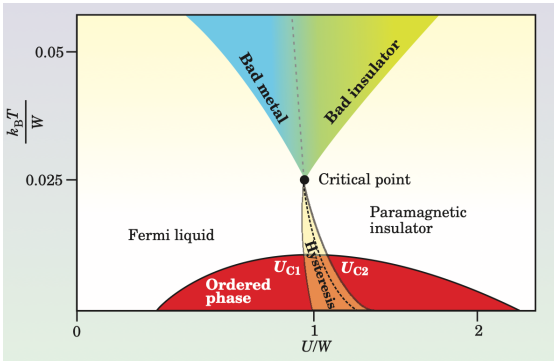

Figure 9. The T vs. U phase diagram of the half-filled Hubbard model as given by DMFT. W is the bandwidth. Figure taken from ref. [24].

finite. Only at $T = 0$ the metallic resistivity is finite whereas the insulating one is infinity. The blueish-greenish region as one goes around the critical point is a region where we have neither a good metal nor a good insulator, the distinction between them being blurred. We call it the "bad metal" or "bad insulator" region. The behavior of the resistivity in this bad metal/insulator region was also obtained within DMFT [31], see Fig. 10(a) . It shows a typical fan-like behavior. It compares well to compounds that exhibit a Mott critical point, as the organic κ-$Cu_2(CN)_3$ [32], see Fig. 10(b)

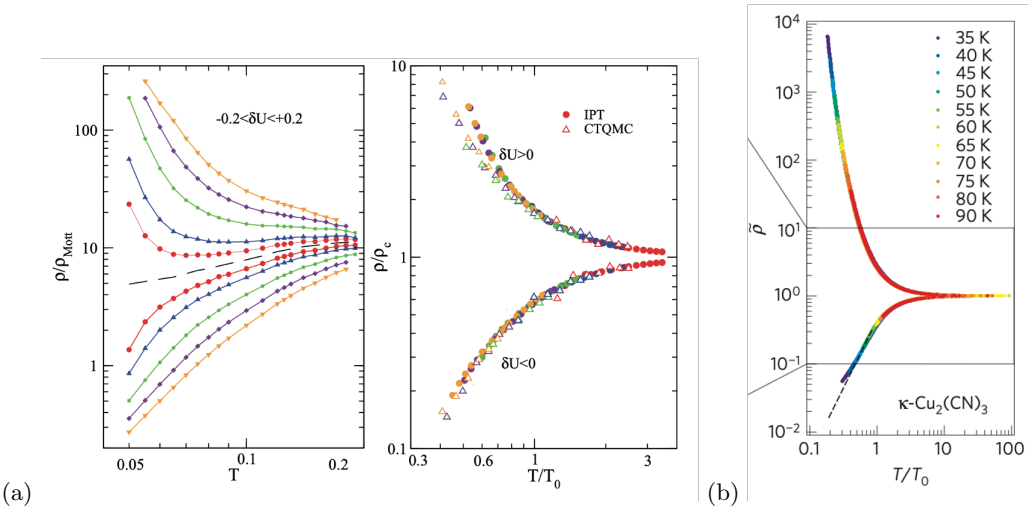

(a) (b)

Figure 10. (a) The resistivity of the half-filled Hubbard model in the bad metal/insulator region, as determined by DMFT. In the bad metal (insulator) region, the resistivity increases (decreases) as the temperature is raised. All the curves can rescaled along the vertical and horizontal axes to fit two universal curves for the metallic and insulating branches. Figure taken from ref. [31]. (b) The resistivity of the organic compound κ-$Cu_2(CN)_3$ close to the Mott critical point. Figure taken from ref. [32].

The red region of Fig. 9 is and antiferromagnetic phase, as expected from the low-energy Heisenberg model description. It can be described within DMFT by defining two sub-lattices A and B and allowing the self-energy to be spin-dependent $\Sigma(\omega) \to \Sigma_\sigma^{A,B}(\omega)$, but otherwise proceeding in similar fashion as described before.

Note that the quasi-particle peak is described by Fermi liquid theory. Therefore, this low-energy sector is the Fermi liquid form of the local Green function of Eq. (26) and its subsequent analysis. But it should never be forgotten that the parameters in that description depend crucially on the self-consistency condition of DMFT. Thus, as U is increased there is a certain critical value above which the self-consistently determined width is zero, Fig. 8(d). This never happens in the single-impurity Anderson model without the additional imposition of the DMFT self-consistency. Remember also that the spectral weight and the renormalized width are governed by the quasi-particle weight Z, see Eqs. (19), (31), (32), and (34). Thus, Z goes to zero above a critical value of U. How does it do so? Since the metal disappears abruptly at the first-order phase transition line, Z goes to zero discontinuously at $U_c(T)$. However, as explained above, the metallic state persists metastably above $U_c(T)$ up until $U_{c2}(T)$. If we follow Z within this

metastable metallic phase,

$$Z \to 0 \;\; \text{as} \; U \to U_{c2}\left(T\right). \tag{47}$$

In the metallic phase, we can use the Fermi liquid form of the self-energy, Eq. (20), and plug it into the lattice Green function of Eq. (40). When we do this, we get at low energies

$$G_{\text{lat}}\left(\mathbf{k},\omega\right) = \frac{Z}{\omega - Z\epsilon_{\mathbf{k}} + i\tilde{\Gamma}}. \tag{48}$$

It is interesting that the dispersion is renormalized by the Z factor. If we expand around the Fermi wave vector

$$\epsilon_{\mathbf{k}} \approx \frac{k_F}{m}\left(k - k_F\right) = v_F\left(k - k_F\right). \tag{49}$$

It follows that the low-energy metallic quasi-particles have a renormalized Fermi velocity v_F^* or, equivalent, effective mass m^* given by

$$v_F \;\; \to \;\; v_F^* = Zv_F, \tag{50}$$

$$m \;\; \to \;\; m^* = \frac{m}{Z}. \tag{51}$$

Thus, as $Z \approx U_{c2}\left(T\right) - U \to 0$ at the metallic spinodal, the effective mass diverges

$$m^* \sim \frac{1}{U_{c2}\left(T\right) - U} \to \infty. \tag{52}$$

III. DMFT PLUS DISORDER

It is possible to adapt DMFT to include the effects of disorder. Consider trying to solve the disordered Hubbard model

$$H_{\text{dis}-\text{Hub}} = \sum_{\mathbf{k},\sigma} \epsilon_{\mathbf{k}} c_{\mathbf{k},\sigma}^{\dagger} c_{\mathbf{k},\sigma} + \sum_{i,\sigma} \varepsilon_i c_{i,\sigma}^{\dagger} c_{i,\sigma} + U \sum c_{i,\uparrow}^{\dagger} c_{i,\uparrow} c_{i,\downarrow}^{\dagger} c_{i,\downarrow}, \tag{53}$$

where ε_i are random site energies describing randomly distributed impurities. We can think of these random variables as chosen from a given distribution function $P\left(\varepsilon\right)$, which we can leave as unspecified for now. I will describe how the DMFT algorithm is modified by the presence of disorder by focusing on physical insight. Once again, a rigorous derivation can be obtained by appealing to the infinite-dimensional lattice.

We start by fixing a certain trial hybridization function $\Delta\left(\omega\right)$ as seen by *every site* of the lattice (it describes the hopping on and off each site). This hybridization function is sort of an *average hybridization*. If we remember that this physics is described by the single-impurity Anderson model, we see that now we have *one impurity problem for each possible value of* $\epsilon_d = \varepsilon_i$. In other words, we have an *ensemble* of impurity problems. Let us assume that we can solve each one of them, by finding the local Green function

$$G_d\left(\varepsilon_i, t - t'\right) = -i\theta\left(t - t'\right)\left\langle \left\{ d_\sigma\left(t\right), d_\sigma^{\dagger}\left(t'\right) \right\} \right\rangle. \tag{54}$$

Since the solution depends on the value of ε_i, we have denoted this by including this dependence in the notation. Likewise, we can find the Fourier transform and local self-energy

$$G_d\left(\varepsilon_i,\omega\right) = \frac{1}{\omega - \varepsilon_i - \Delta\left(\omega\right) - \Sigma\left(\varepsilon_i,\omega\right)}, \tag{55}$$

where we again made explicit the ε_i-dependence in the notation.

It is clear now that we should make some assumption to connect the local problem to the lattice problem. The DMFT procedure assumes the existence of an *effective medium self-energy* $\Sigma_{\text{EM}}\left(\omega\right)$. It can be obtained by *averaging the local Green function*

$$\overline{G_d\left(\omega\right)} = \int d\varepsilon \frac{P\left(\varepsilon\right)}{\omega - \varepsilon - \Delta\left(\omega\right) - \Sigma\left(\varepsilon,\omega\right)} = \frac{1}{\omega - \Delta\left(\omega\right) - \Sigma_{\text{EM}}\left(\omega\right)}. \tag{56}$$

Now, this effective medium self-energy is the *same one* affecting lattice propagation

$$G_{\text{lat}}(\mathbf{k},\omega)=\frac{1}{\omega-\epsilon_{\mathbf{k}}-\Sigma_{\text{EM}}(\omega)}, \tag{57}$$

so the local lattice Green function is given by

$$\overline{G_{\text{lat}}(\mathbf{0},\omega)}=\sum_{\mathbf{k}}\overline{G_{\text{lat}}(\mathbf{k},\omega)}=\sum_{\mathbf{k}}\frac{1}{\omega-\epsilon_{\mathbf{k}}-\Sigma_{\text{EM}}(\omega)}. \tag{58}$$

Finally, the self-consistency condition comes from equating the two forms of the average local Green function

$$\int d\varepsilon\frac{P(\varepsilon)}{\omega-\varepsilon-\Delta(\omega)-\Sigma(\varepsilon,\omega)}=\sum_{\mathbf{k}}\frac{1}{\omega-\epsilon_{\mathbf{k}}-\Sigma_{\text{EM}}(\omega)}. \tag{59}$$

Obviously, in the limit of zero disorder, $\Sigma(\varepsilon,\omega)\to\Sigma(\omega)=\Sigma_{\text{EM}}(\omega)$. The self-consistency loop now read:

1. Start with an initial guess for the hybridization function $\Delta(\omega)$.
2. Solve the *ensemble of impurity problems* using some impurity solver to find $G_d(\varepsilon_i,t-t')=-i\theta(t-t')\left\langle\left\{d_\sigma(t),d_\sigma^\dagger(t')\right\}\right\rangle$.
3. Obtain its Fourier transform $G_d(\varepsilon_i,\omega)$.
4. Average $G_d(\varepsilon_i,\omega)$ over ε_i to find $\overline{G_d(\omega)}$ [first equality of Eq. (56)], and then obtain the effective medium self-energy from $\Sigma_{\text{EM}}(\omega)=\omega-\Delta(\omega)-\left[\overline{G_d(\omega)}\right]^{-1}$ [second equality of Eq. (56)].
5. Use the effective medium self-energy to get the average local lattice Green function
$$\overline{G_{\text{lat}}(\mathbf{0},\omega)}=\sum_{\mathbf{k}}\frac{1}{\omega-\epsilon_{\mathbf{k}}-\Sigma_{\text{EM}}(\omega)}. \tag{60}$$
6. Obtain a new hybridization function from solving [Eq. (59)]
$$\int d\varepsilon\frac{P(\varepsilon)}{\omega-\varepsilon-\Delta_{\text{new}}(\omega)-\Sigma(\varepsilon,\omega)}=\overline{G_{\text{lat}}(\mathbf{0},\omega)}. \tag{61}$$
Note that this last equation looks complicated but it can be solved separately for each value of ω (different ω-values do not mix), so it is not so bad.
7. Test if $\Delta_{\text{new}}(\omega)=\Delta(\omega)$. If yes, self-consistency has been reached. If not, use $\Delta_{\text{new}}(\omega)$ as the new hybridization function and go back to step 1.

A few words must be said about the DMFT treatment of disorder plus interactions. Although it contains rich and interesting physics, as we will explore, it also has the limitation that it does not describe the disorder-induced Anderson localization transition. We will talk more about this later, but remember that Anderson localization is not captured within DMFT. If only disorder is concerned, the description provided by DMFT is equivalent to the so-called Coherent Potential Approximation (CPA) [see [33], pg. 154], which is important but is not able to describe Anderson localization. However, there is an extension of DMFT that does capture Anderson localization. More about this later.

A. Effects of disorder on the Mott-Hubbard transition

Some effects from the DMFT treatment of the disordered Hubbard model were obtained in refs. [34, 35], which focused on the $T=0$ and $T\neq 0$ behaviors, respectively. We will highlight the most important results.

The $T=0$ phase diagram at half-filling is seen in Fig. 11(a). The Mott-Hubbard insulator is suppressed by disorder, as expected, since impurity states will appear inside the Mott gap, eventually filling it up. This is shown by the full line in the phase diagram. The other dotted and dashed lines are different estimates of the boundary between the strongly correlated metal and the disorder-driven Anderson insulator, whose description is beyond DMFT. We will return to this topic later.

At this point, it is useful to look at the local Green function of Eq. (55) in the low-energy metallic Fermi liquid regime, in which we can use the parametrization of Eqs. (20) and (21), modified to exhibit site-dependent parameters

$$\begin{aligned} G_d\left(\varepsilon_i, \omega \approx 0\right) &= \frac{1}{\omega - \varepsilon_i - \Delta\left(\omega\right) - \Sigma\left(\varepsilon_i, \omega\right)} \\ &\approx \frac{Z_i}{\omega - Z_i\left[\varepsilon_i + \Delta'\left(0\right) + \delta_i\right] + iZ_i\left[\Delta''\left(0\right) + \Gamma_i\right]}. \end{aligned} \tag{62}$$

This form gives rise to local Kondo resonances, one at each site. The approach to the transition line is signaled by the vanishing of all quasi-particle weights (strictly at $T = 0$, there is only a second-order phase transition point), and hence of all the local Kondo resonances

$$Z_i \to 0 \text{ as } U \to U_c\left(W\right). \tag{63}$$

But now recall the phenomenon of Fermi level pinning, expressed by Eq. (29) (note that the appearance of a random on-site energy ε_i does not kill the effect), which acts to center each resonance on the Fermi level

$$Z_i\left(\varepsilon_i + \Delta'\left(0\right) + \delta_i\right) \approx 0. \tag{64}$$

Thus, the bare disorder potential ε_i is effectively suppressed to a minute renormalized value $\varepsilon_i + \Delta'\left(0\right) + \delta_i \approx 0$, a phenomenon called disorder screening by strong correlations. The screening is the stronger the closer to the transition line, because of the decrease of the Z_i. Note that this only happens at low energies. At higher energies this is ineffective and the effect of disorder is much larger. At higher energies, the physics of the Hubbard bands comes into play and they are not screened. It follows that, using Eq. (56), the average self-energy, $\Sigma_{\mathrm{EM}}\left(\omega\right)$, can be determined. Now, the average self-energy, which also appears in the lattice Green function, see Eq. (57), is the ingredient necessary for the calculation of the system's electric resistivity [23], more specifically its imaginary part gives the scattering rate, which is proportional to the resistivity

$$\frac{1}{\tau} = 2\mathrm{Im}\Sigma_{\mathrm{EM}}\left(\omega = 0\right). \tag{65}$$

As seen in Fig. 11(b), disorder screening at large U leads to a dramatic suppression of the scattering rate.

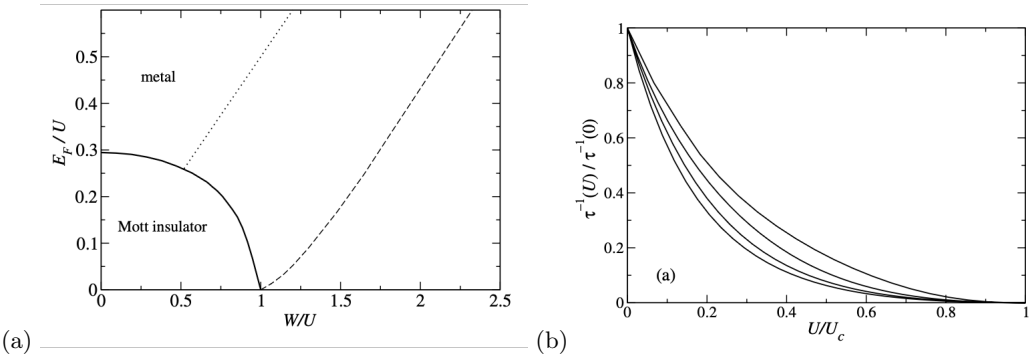

Figure 11. (a) The $T = 0$ phase diagram of the half-filled disordered Hubbard model, as given by DMFT. Here, E_F is the Fermi energy (equal to the half band-width D in the clean case) and W is the disorder strength. The full line delineates the metal-Mott-insulator transition and the dotted and dashed lines are two estimates of metal-Anderson-insulator transition. (b) Scattering rate as a function of U, for different values of disorder (increasing upwards), showing the effect of disorder screening by strong correlations. Figures taken from ref. [34].

The T vs. U phase diagram for several values of disorder [35] is shown in Fig. 12 (a). Two important features are worth mentioning. First, the coexistence region shifts to higher U values and shrinks with the increase of disorder. The effect of disorder is to broaden the bandwidth and to introduce impurity states inside the gap. Thus, larger values of U are required to establish the Mott gap.

Additionally, the phenomenon of disorder screening by strong correlations survives at low, yet non-zero temperatures, where Fermi liquid theory still applies. The average spectral function (imaginary part of the Eq. (56)) as function of frequency is shown in Fig. 12 (b) in the left-hand panel, while its the relative fluctuations are shown in the right-hand panel. The fluctuations are small at low ω, but reach much higher values for larger frequencies.

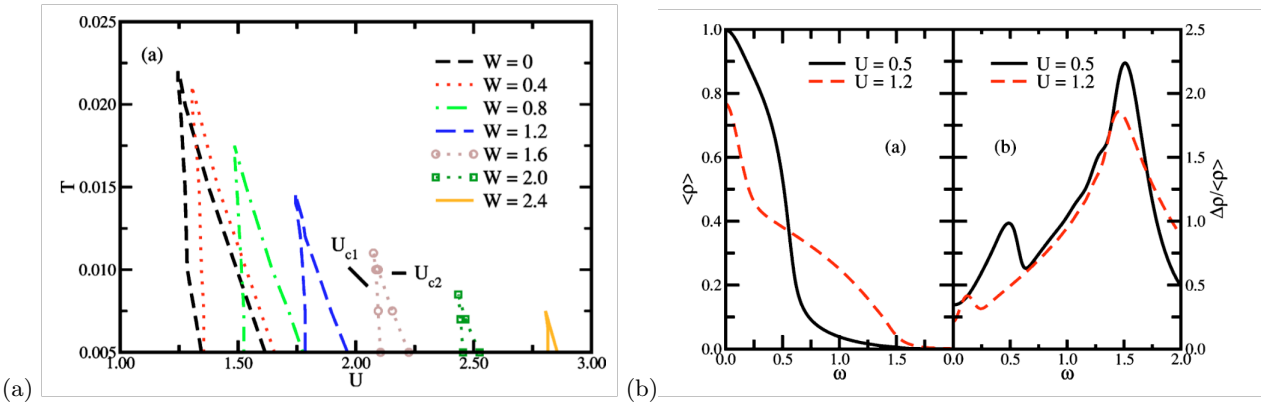

Figure 12. (a) The T vs. U phase diagram of the half-filled disordered Hubbard model, as given by DMFT, for various levels of disorder strength. The band-width is the energy unit. (b) Average local density of states (left-hand panel) and its relative fluctuations (right-hand side), showing disorder screening at low energies, for $T = 0.005$ and $W = 1.0$. Figures taken from ref. [35].

IV. KONDO DISORDER

The concept of Kondo disorder is one where the framework of DMFT plus disorder and its generalizations gained some traction. Roughly speaking, the *ensemble* of single-impurity problems that underlie the formalism suggests the interesting question: What is the physics of a system with a distribution of Kondo temperatures? More specifically, the low-energy behavior of the *ensemble* of local Green functions of Eq. (62) naturally leads to site-dependent Kondo temperatures once we generalize Eq. (31) to include disorder

$$T_{Ki} = \tilde{\Delta}_i''(0) = Z_i \Delta''(0). \tag{66}$$

The important question is how does the introduction of the concept of a distribution of Kondo temperatures impacts both thermodynamic (specific heat, magnetic susceptibility) and transport (resistivity) properties?

In the context of the disordered Hubbard model, the spatial fluctuations of T_K come about because the local on-site energy ε_i acts like the d-level energy of the single-impurity problem and the Kondo temperature is affected through the Kondo coupling

$$T_{Ki} = D \exp\left(-\frac{1}{\rho_F J_{Ki}}\right), \tag{67}$$

$$J_{Ki} = 2V^2\left(\frac{1}{\varepsilon_i + U} - \frac{1}{\varepsilon_i}\right). \tag{68}$$

In this case, since the local environment seen by the particular site is always the same [they all see the same $\Delta(\omega)$], there are no fluctuations in either D or ρ_F.

However, a lot of the discussion around Kondo disorder, particularly as related to experiments, revolved around a different model, the disordered *Anderson lattice model*. It is a straightforward generalization of the Anderson single-impurity model to account for a situation where you have a dense lattice of local moments, particularly one per unit cell. In other words, the concentration of dilute random impurities is increased to the limit where there is one per unit cell, in which case it does not make sense to call them either dilute or impurities. The Hamiltonian describing this state of affairs is, in the clean limit,

$$H_{\text{AndLatt}} = \sum_{\mathbf{k},\sigma} \epsilon_{\mathbf{k}} c^\dagger_{\mathbf{k},\sigma} c_{\mathbf{k},\sigma} + \sum_{i,\sigma} E_f f^\dagger_{i\sigma} f_{i\sigma} + \sum_{i,\sigma} V\left(c^\dagger_{i,\sigma} f_{i\sigma} + f^\dagger_{i\sigma} c_{i,\sigma}\right) + U \sum_i f^\dagger_{i\uparrow} f_{i\uparrow} f^\dagger_{i\downarrow} f_{i\downarrow}, \tag{69}$$

where we switched the d-operators to f-operators, as most of the systems of interest now have incomplete $4f$- or $5f$-shells (typically from the rare-earth or actinide elements Ce, U, Yb, Sm, Pr). Note that we wrote the hybridization in the site basis, imagining the situation of one f-orbital per c-orbital.

The formalism of DMFT, with or without disorder, can be easily generalized to the Anderson lattice model. We will not go into more detail about this generalization, which can be found in ref. [36], but we will appeal to the physical

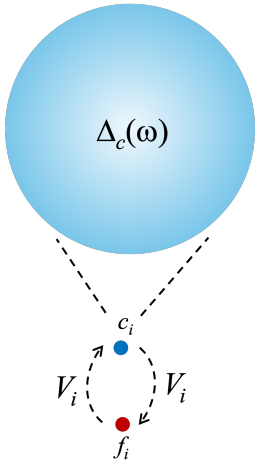

Figure 13. Schematic depiction of the DMFT theory of the disordered Anderson lattice. Each site is composed of one c- and one f-orbital. The c-orbital "sees" the rest of the lattice through the self-consistently determined function $\Delta_c(\omega)$, which, however, does not have spatial fluctuations.

intuition acquired from the discussion of the Hubbard model. First let us introduce disorder in the Anderson lattice model

$$H_{\mathrm{dis-AndLatt}} = \sum_{\mathbf{k},\sigma} \epsilon_{\mathbf{k}} c^{\dagger}_{\mathbf{k},\sigma} c_{\mathbf{k},\sigma} + \sum_{i,\sigma} \varepsilon_i c^{\dagger}_{i,\sigma} c_{i,\sigma} + \sum_{i,\sigma} E_{fi} f^{\dagger}_{i\sigma} f_{i\sigma} + \sum_{i,\sigma} V_i \left(c^{\dagger}_{i,\sigma} f_{i\sigma} + f^{\dagger}_{i\sigma} c_{i,\sigma} \right) + U \sum_i f^{\dagger}_{i\uparrow} f_{i\uparrow} f^{\dagger}_{i\downarrow} f_{i\downarrow}. \quad (70)$$

Note that we have introduced disorder in the conduction electron sites, in the energy of the f- level (there might be different elements like Ce and La, for example), and in the hybridization amplitude (different c- or f-orbitals will surely hybridize in different ways). One might even have different U values (for different elements with incomplete f-shells) but we will disregard this possibility here.

The important point in the DMFT treatment of the disordered Anderson lattice is that in each unit cell there is an individual (i.e. spatially fluctuating) c- and an f-orbital, but the c-orbital "sees" the rest of the lattice through a unique, self-consistently determined, average environment described by the hybridization function $\Delta_c(\omega)$. Thus, once self-consistency is reached, the unit cells define an *ensemble* of single-impurity problems, each characterized by a set of parameters $(E_{fi}, V_{i,})$ *and a hybridization function* given by

$$\Delta_{fi}(\omega) = \frac{V^2}{\omega - \varepsilon_i - \Delta_c(\omega)}. \quad (71)$$

Note that we were careful to define two hybridization functions, $\Delta_c(\omega)$ for the conduction electrons, that is an average value that does not fluctuate, and $\Delta_{fi}(\omega)$ for the f-electrons that does fluctuate spatially through ε_i.

Thus, the local Kondo temperature has now several sources of spatial fluctuations and we may write

$$T_{Ki} = D \exp\left(-\frac{1}{\rho_{Fi} J_{Ki}} \right), \quad (72)$$

$$J_{Ki} = 2V_i^2 \left(\frac{1}{E_{fi} + U} - \frac{1}{E_{fi}} \right), \quad (73)$$

where even the density of states of the conduction electrons is not the same in each unit cell. Given the bare distributions of the parameters in the Hamiltonian, $P_f(E_f)$, $P_V(V)$,and $P_c(\varepsilon)$, we can, in principle, find the self-consistent solution of the DMFT equations and the corresponding distribution of Kondo temperatures $P(T_K)$.

In any case, the question is: what are the physical consequences of a distribution of Kondo temperatures? DMFT once again gives well-defined answers. For thermodynamic quantities, deep in the paramagnetic phase and away from magnetic ordering of any kind, the *ensemble* of impurity problems responds quite independently from one another and the overall behavior can be taken to be the average of the thermodynamic quantity in question. Thus, for example, we can write the system's magnetic susceptibility as

$$\chi(T) = \int dT_K P(T_K) \chi(T, T_K), \quad (74)$$

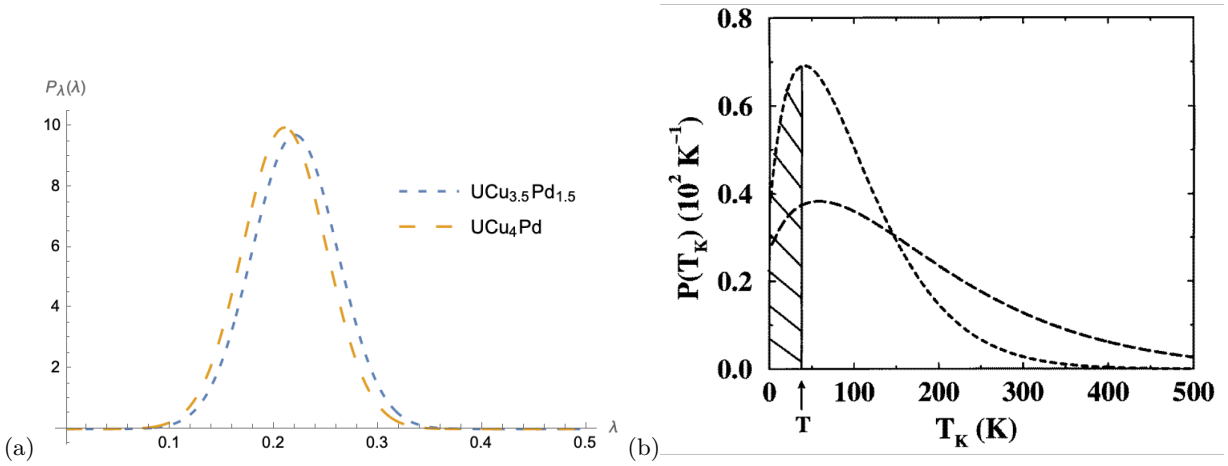

Figure 14. Experimentally inferred distributions of (a) $\lambda_i \equiv \rho_{Fi} J_{Ki}$ and (b) Kondo temperatures for the alloys $UCu_{5-x}Pd_x$, with $x = 1.5$ (short-dashed line) and 1 (long-dashed line). The ratio of the standard deviation to the average of λ is small in both cases ($\Delta\lambda/\lambda_{\rm av} \approx 0.19$), but the distributions of T_K are much broader. Figure of $P\left(T_K\right)$ taken from reference [37].

where $\chi\left(T, T_K\right)$ is the susceptibility of a single-impurity problem with Kondo temperature T_K. The susceptibility $\chi\left(T, T_K\right)$, on the other hand, has a universal form, see Fig. 4 and the discussion around Eq. (12). It has a fairly accurate parametrization given by [10]

$$\chi\left(T, T_K\right) \sim \frac{1}{T + \alpha T_K}, \tag{75}$$

where α is a universal number or order 1. A very interesting result now ensues if the distribution $P\left(T_K\right)$ has some special features.

First note the strong exponential dependence of the Kondo temperature on the parameters, Eqs. (72) and (73). Thus, even for moderate disorder of the microscopic parameters $(\varepsilon_i, V_i, \rho_{Fi})$ very large distributions of Kondo temperatures can ensue. Take, for example, the distributions inferred from magnetic susceptibility and nuclear magnetic resonance experiments on the alloys $UCu_{5-x}Pd_x$ ($x = 1$ and 1.5) shown in Fig. 14. The distributions of the quantity inside the exponential of the Kondo temperature of Eq. (72), $\lambda_i \equiv \rho_{Fi} J_{Ki}$, are quite narrow: the ratio of the standard deviation to the average value of λ is fairly small in both cases ($\Delta\lambda/\lambda_{\rm av} \approx 0.19$), as can be seen Fig. 14(a). Nevertheless, the widths of the T_K distributions are much larger, as shown in Fig. 14(b).

The first feature that catches the eye is the fact that

$$P\left(T_K \to 0\right) \to \text{const.} \tag{76}$$

This is has deep consequences for the physical behavior. Indeed, plugging this kind of distribution into Eq. (74) and using Eq. (75) we get

$$\begin{aligned} \chi\left(T\right) &= \int dT_K P\left(T_K\right) \chi\left(T, T_K\right) \\ &= \int dT_K \frac{P\left(T_K\right)}{T + \alpha T_K}. \end{aligned} \tag{77}$$

Now, to get the leading low-temperature behavior of $\chi\left(T\right)$, we notice that, as $T \to 0$, the integral is dominated by the $T_K \approx 0$ region, which is singular if $P\left(T_K \to 0\right) \to$ const., as it does. We thus cut the integral at a low-energy cutoff Λ, since the contribution for $T_K > \Lambda$ is regular and sub-leading,

$$\begin{aligned} \chi\left(T\right) &\sim \int_0^\Lambda dT_K \frac{P\left(T_K\right)}{T + \alpha T_K} \\ &\sim \int_0^\Lambda dT_K \frac{P_0 + P_1 T_K}{T + \alpha T_K} \\ &\sim P_0 \ln\left(\frac{\Lambda + T}{T}\right) + P_1 \left[\Lambda - T \ln\left(\frac{\Lambda + T}{T}\right)\right] \end{aligned}$$

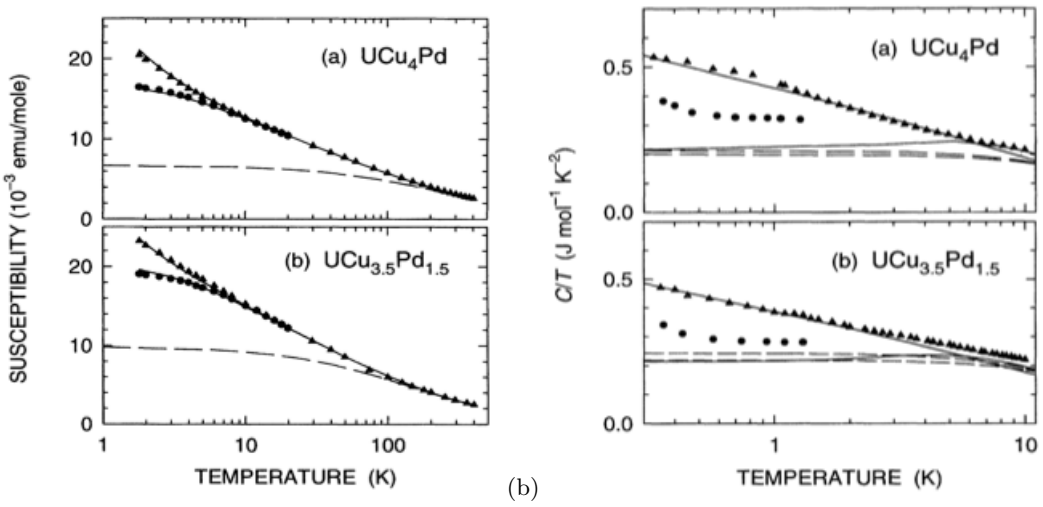

Figure 15. (a) Magnetic susceptibility of $UCu_{5-x}Pd_x$ at $H = 5$ kOe (triangles) and $H = 5$ kOe (circles); (b) Specific heat divided by temperature of $UCu_{5-x}Pd_x$ at $H = 0$ (triangles) and $H = 140$ kOe (circles). Figures taken from ref. [39].

$$\begin{aligned} &\sim P_0 \ln\left(\frac{\Lambda}{T}\right) + P_1\Lambda + \mathcal{O}\left(T, T\ln\left(\frac{\Lambda}{T}\right)\right) \\ &\sim P_0 \ln\left(\frac{\tilde{\Lambda}}{T}\right). \end{aligned} \tag{78}$$

The leading low-temperature behavior for a distribution such that $P(T_K \to 0) \to$ const. is a logarithmic divergence. Since this is at odds with the behavior of a normal Fermi liquid ($\chi(T) \sim$ const.), this is described as *non-Fermi liquid behavior*. This is a striking result of the Kondo disorder model. The same kind of log-divergence is obtained for the specific heat divided by the temperature, $C(T)/T$. Both behaviors are indeed seen in $UCu_{5-x}Pd_x$, see Fig. 15, and several other disordered materials [38].

Physically, we can look at Fig. 14 and argue that, at a certain temperature T, as indicated in the figure, the spins can be separated into two sets. Those that have $T_K \gg T$, whose contribution to the integral in Eq. (77) is small, and those that have $T_K \ll T$ (hatched area in Fig. 14), whose contribution to Eq. (77) is very large if $T \to 0$. The boundary spins give a non-singular, regular contribution. Thus, as $T \to 0$, the average susceptibility is *dominated by only a few low-T_K spins*, a phenomenon that goes under the general heading of "rare-event" physics. This kind of rare-event dominated average is a regular feature of several effects present in disordered systems, as we will see later on.

Note that, for small disorder, we expect there to be a narrow distributions of T_K's that goes to zero fast as $T_K \to 0$. Effectively, we can think of a lower bound $T_{K\min}$, so that, for $T \ll T_{K\min}$, only large-T_K spins contribute to the average of Eq. (77), which will give regular Fermi liquid behavior

$$\chi(T) \sim \text{const.} \tag{79}$$

It is clear that non-Fermi liquid behavior requires a sufficiently large amount of disorder.

It is interesting to inquire what this picture implies for the resistivity. The resistivity can also be calculated within disordered DMFT. The reasoning is more complicated, though, because transport is not simply additive as thermodynamics. Indeed, one of the hallmarks of clean systems with a lattice of f-derived local moments (so-called heavy fermion materials) is the onset of coherence at low temperatures. This is nicely illustrated in Fig. 16. In the (a) panel, the resistivity of a single (or a few dilute) magnetic impurity(ies) is shown. The resistivity increases as the temperature is decreased but it saturates to a constant large value at $T = 0$. This is called Kondo scattering, as it is corresponds to the Kondo model of Eq. (9). Analysis shows that the resistivity at low T is maximum, corresponding to the so-called unitary scattering, with phase shift $\delta_0 = \pi/2$. Indeed, the dilute limit of the $Ce_xLa_{1-x}Cu_6$ alloy of Fig. 16(b), with $x = 0.094$, is very much like that. Here, the Ce^{3+} ions are the magnetic elements. As one increases the concentration of Ce ions, roughly the same sort of behavior is seen, but something rather different happens when one reaches the limit of $x = 1$, where the Ce ions form a periodic lattice. In that limit, strong Kondo scattering becomes coherent and the resistivity has a sharp drop, finally settling to very small values at the lowest temperatures. It is clear that the resistivity is not additive as the susceptibility or the specific heat. Indeed, DMFT calculations are able to capture the low-temperature coherence of heavy-fermion materials.

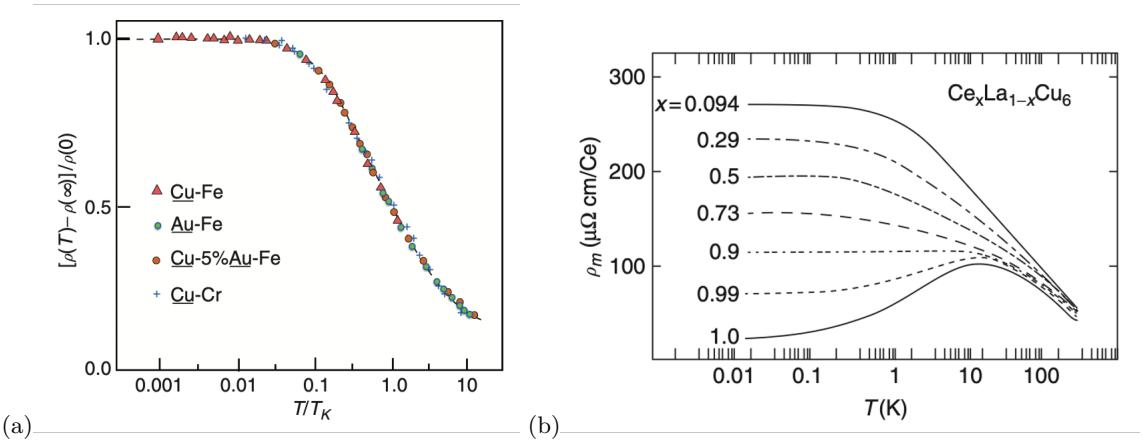

Figure 16. (a) Resistivity of dilute magnetic impurities in normal metals showing typical Kondo scattering, where resistivity increases with decreasing temperatures and saturates at the lowest temperatures; (b) Resistivity of a series of $Ce_xLa_{1-x}Cu_6$ alloys, from the dilute limit ($x = 0.094$) up to the stoichiometric limit $x = 1$ of the heavy fermion material $CeCu_6$. For most values of x, there is typical Kondo scattering. Close to stoichiometry, though, the large scattering at high and intermediate temperatures is followed by low-temperature coherence and good metallic resistivity. Figures 16.19 and 17.3 from ref. [40].

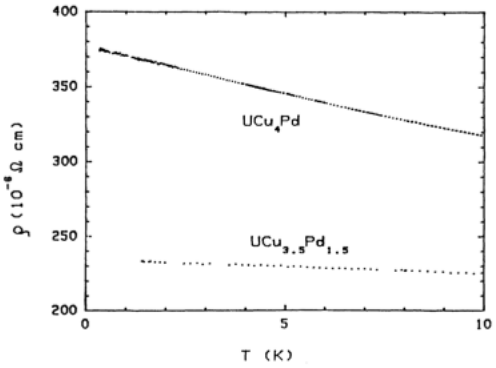

Figure 17. Resistivity of $UCu_{5-x}Pd_x$. Figure taken from ref. [41].

The question is what happens when we strongly disorder the lattice, as in the $UCu_{5-x}Pd_x$ alloys discussed above. Two important things happen. First, enough disorder can completely destroy coherence and lead to a large residual resistivity as in the case of Fig. 16(b), with x up to $x = 0.9$. But more importantly, the deviation from $T = 0$ assumes a non-Fermi liquid form

$$\rho(T) = \rho(0) - AT, \tag{80}$$

with a linear temperature dependence with a negative coefficient. This linear behavior can also be understood with a simple physical argument (the detailed calculation confirms this argument). At $T = 0$, all the Kondo scatterers are at their zero-temperature unitary limit of strong scattering. If the temperature is raised a small amount T, a few scatterers will have $T_K \ll T$, see the hatched area of Fig. 14. The "high-temperature" Kondo scattering is very small at those few sites, see Fig. 16(a). Thus, the overall incoherent scattering will **decrease** by an amount proportional to the density $n_{\text{low}-T_K}$ of those low-T_K sites. Thus

$$\Delta\rho(T) = \rho(T) - \rho(0) \propto -n_{\text{low}-T_K} \propto -P(0) \times T. \tag{81}$$

This behavior is indeed observed in $UCu_{5-x}Pd_x$, see Fig. 17, and other disordered materials [38].

V. QUASI-CRYSTALS

It is interesting to see the results of the Kondo disorder concept in a different but somewhat related context: local moments in quasi-crystals. Quasi-crystals exhibit non-disordered, yet non-periodic lattices. A well known example

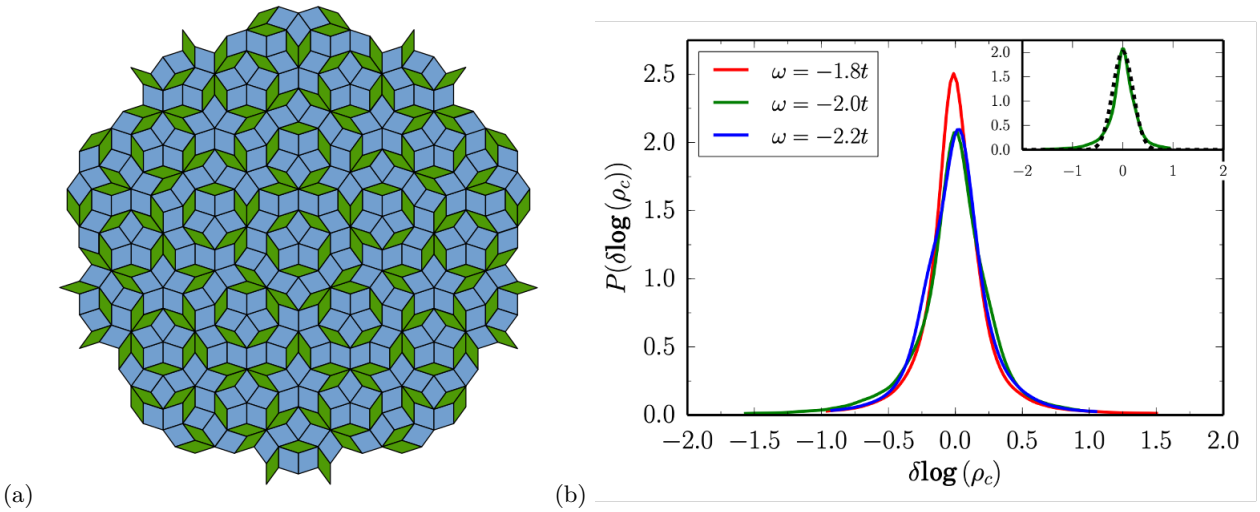

Figure 18. (a) The Penrose tiling of the two-dimensional plane by two kinds of rhombuses. Figure taken from Wikipedia; (b) Distribution of local densities of states in an octogonal quasi-crystal. Figure taken from ref. [42].

of this type of lattice is the famous Penrose tiling of the two-dimensional plane by two kinds of rhombuses, as shown in Fig. 18. Note how (i) the pattern never repeats itself and (ii) some vertices have a 5-fold coordination, which is rigorously forbidden in a periodic tiling of the plane.

Now, the electronic states on a quasi-crystalline lattice do not obey Bloch's theorem. Therefore, they are not completely extended states, but more commonly exhibit power-law envelope decay, being sort of intermediate between exponentially localized states, characteristic of Anderson localized states by disorder, and extended Bloch states. Besides, the local environment of any lattice site is never the same, due to the complete lack of periodicity. Therefore, an interesting question arises. Suppose we put a localized spin at each vertex of a quasi-crystal. Since the local environment fluctuates, we expect fluctuations of the hybridization function $\Delta_i(\omega)$, which, we recall, describes how the local moment "sees" the rest of the lattice. So, even if all the spins are the same and couple equally to the local environment, we expect a distribution of Kondo temperatures. Indeed if we refer back to Eq. (72), even though J_{Ki} may be the same for every spin, the local density of states ρ_{Fi} will fluctuate spatially and give rise to a Kondo temperature distribution. This is indeed what was found [42]. It was found that the distribution of Kondo temperatures shows a power-law form

$$P(T_K) \sim T_K^{\alpha-1}, \tag{82}$$

with a non-universal exponent α that depends on the value of J_K. This is shown in Fig. 19(a) for various values of J_K. The linear behavior at low T_K indicates the power-law form in a log-log plot. Correspondingly, through Eq. (77), this leads to a power-law behavior of the magnetic susceptibility $\chi(T) \sim T^{\alpha-1}$, as shown in Fig. 19(b). If $\alpha < 1$, the susceptibility diverges at low T ($\alpha = 1$ gives a log-divergence). It is interesting to note what happens if instead of an infinite quasi-crystal, one investigates a so-called approximant, which is a periodic repetition of a chunk of a quasi-crystal. In that case, because the number of local environments is finite, there will always be a lowest Kondo temperature $T_{K\min}$, below which the susceptibility saturates to a finite value, see Eq. (75). This is indeed what is found, see the inset of Fig. 19(b), where the susceptibility of an approximant made of a chunk of an $N_a = 7$-site quasi-crystal is compared to an essentially infinite quasi-crystal ($N_a = 1393$).

Interestingly, there are indeed quasi-crystalline materials with local moments. One example is $Au_{51}Al_{34}Yb_{15}$, where the Yb ions have a well-defined local moment. The magnetic susceptibility of these quasi-crystals shows a power-law divergence [43], as seen in Fig. 20. Approximants of the perfect quasi-crystals can also be grown, and these do not show the divergence down to $T = 0$, see the inset of Fig. 20. Since this is a dense lattice of magnetic ions, it is unclear if the Kondo disorder idea is enough to explain the phenomenology of these materials. Indeed, the specific heat divided by T, $C(T)/T$, should show the same power-law behavior as $\chi(T)$, but is just log-divergent. Although there may be more to the story of the physics of these compounds, it is clear that the concept of a distribution of Kondo temperatures is part of the explanation.

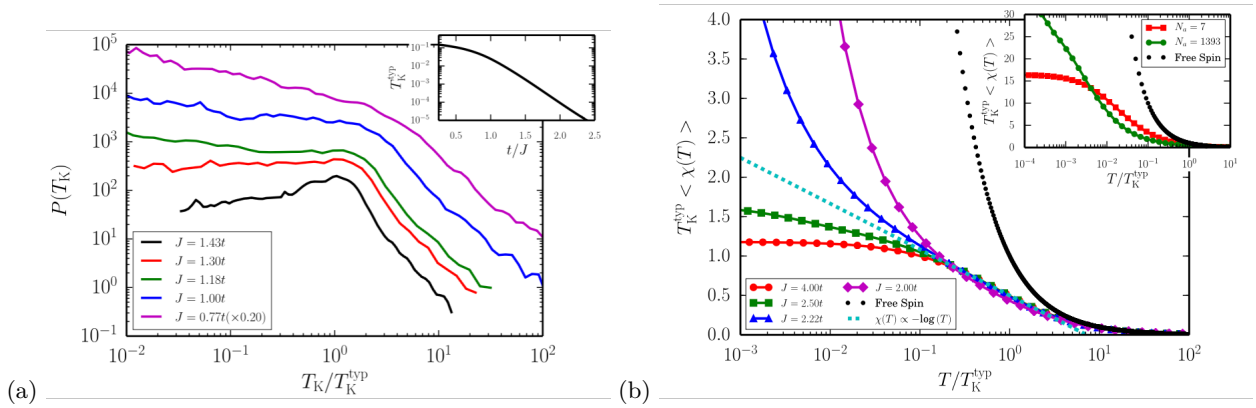

Figure 19. (a) Distribution of Kondo temperatures for an octogonal quasi-crystal for different values of J_K, showing a power-law behavior; (b) The corresponding magnetic susceptibility of the quasi-crystal, which also follows a power law. Figures taken from ref. [42].

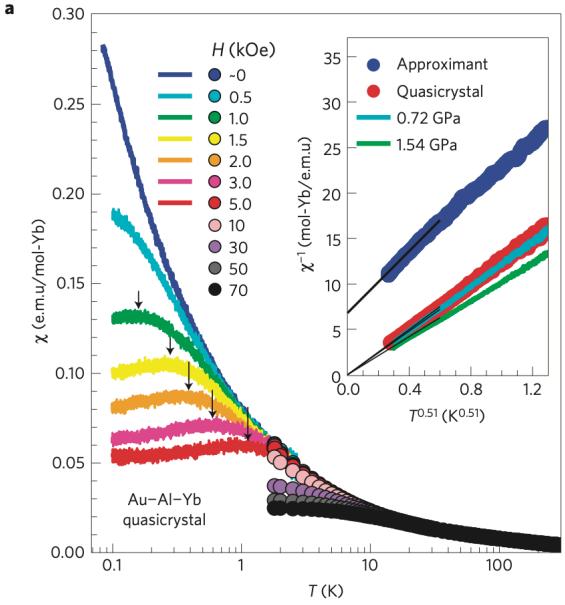

Figure 20. The magnetic susceptibility of the quasi-crystal $Au_{51}Al_{34}Yb_{15}$ for various values of magnetic field. The $H = 0$ limit shows a power-law divergence $\chi(T) \sim T^{-0.51}$. In contrast, the susceptibility of the approximant (blue circles of the inset) saturates to a finite value as $T \to 0$. Figure taken from ref. [43].

VI. THE ANDERSON METAL-INSULATOR TRANSITION

One of the most important phenomena of disordered systems is the Anderson localization of single-particle states [44]. So, before we proceed, let us briefly describe the central ingredients of Anderson localization. We know, from Bloch's theorem, that quantum states in a periodic potential are extended, in the sense that the probability $|\psi_{\mathbf{k}}(\mathbf{r})|^2$ is finite throughout the lattice. If we now introduce some disorder say, by adding a random potential to the periodic one, $\mathbf{k}$ will no longer be a good quantum number (not conserved), but the complex-squared wave function will still be finite throughout the lattice. What happens as we keep on increasing the disorder? Let us be more quantitative and define a lattice tight-binding model with disorder, for definiteness, just like we did for the Hubbard model in Eq. (53), but turning off the interactions (this is yet another Anderson Hamiltonian: do not lose count!)

$$H_{\text{And}} = -t \sum_{\langle i,j\rangle,\sigma} \left(c^\dagger_{i,\sigma} c_{j,\sigma} + \text{h.c.} \right) + \sum_{i,\sigma} \varepsilon_i c^\dagger_{i,\sigma} c_{n,\sigma}, \tag{83}$$

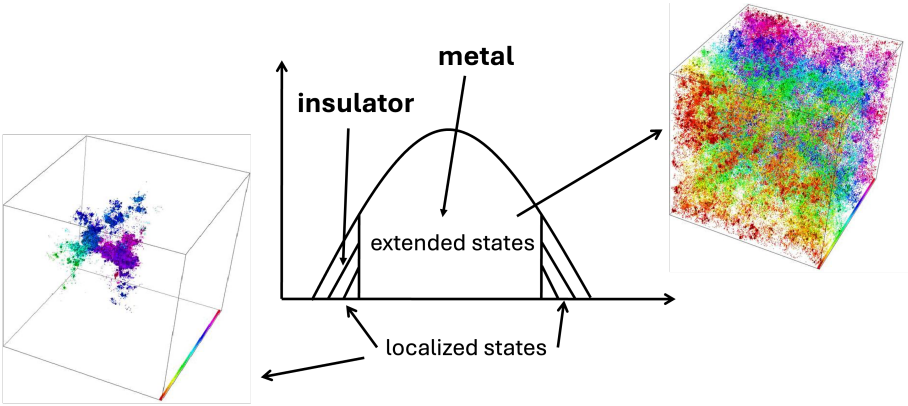

Figure 21. The band of states of a disordered system separates into extended states in the middle region, whose complex-squared wave functions extend throughout the system, and localized states on both the low- and high-energy sides (hatched areas), which occupy only a finite region of the systems. In the side figures we see colored representations of $|\psi_n(\mathbf{R}_i)|^2$ from a calculation of eigenstates of the Anderson Hamiltonian of Eq. (83). Figures of complex-squared wave functions taken from ref. [45].

where each ε_i is identically and independently distributed according to some given distribution $P(\varepsilon)$. We can quantify the amount of disorder by the width of the distribution, given, for example by the standard deviation

$$W = \sqrt{\overline{\varepsilon^2} - (\overline{\varepsilon})^2}, \tag{84}$$

where an overbar denotes an average taken with the distribution $P(\varepsilon)$

$$\overline{f(\varepsilon)} = \int P(\varepsilon) f(\varepsilon) d\varepsilon. \tag{85}$$

What Anderson showed was that for a sufficiently large W compared to the bandwidth $2D$, the states become localized, in the sense that their complex-squared wave function is finite only in a finite region of space centered at some point $\mathbf{R}_c$, but decays exponentially to zero with the distance to that point

$$|\psi_n(\mathbf{R}_i)|^2 \sim \exp(-|\mathbf{R}_i - \mathbf{R}_c|/\xi), \tag{86}$$

where ξ is the so-called localization length, that measures the "size" of the wave function, see the colored representation of $|\psi_n(\mathbf{R}_i)|^2$ on the left-hand side of Fig. 21.

Localization in a lattice system as the one described by the Hamiltonian of Eq. (83) is actually such that, for intermediate values of disorder, the states can be either localized or extended, depending on their energy. The states in the middle region of the band are extended and the states on the low- and high-energy sides of the band are localized, see the schematic plot in Fig. 21. There are two sharp energy values separating the localized states from the extended ones, called "mobility edges". As energies tend to the mobility edges, the localization length diverges, a feature characteristic of second-order phase transitions. As the disorder W is increased, the band of extended states disappears when a critical disorder strength W_c is reached and all the states become localized, see Fig. 22.

The ground state of the fermionic system is constructed by filling up states up to the Fermi level. If the Fermi level lies in the localized state region, the system is an Anderson insulator, as current cannot flow from one side of the sample to the other through localized states. If the Fermi level lies in the extended state region we have a dirty metal. If we can tune the chemical potential (Fermi level at $T = 0$) across the mobility edge, there is a metal-Anderson insulator transition with the $T = 0$ conductivity going to zero right at the mobility edge. It is a 2nd-order phase transition. A transition at first sight compatible with this phenomenology has indeed been observed in doped semiconductors, as shown in Fig. 23.

Microscopically, Anderson showed that one way of characterizing the metal-insulator transition is by looking at the local density of states (DOS) at a generic site $\mathbf{R}_i$, defined by

$$\rho(\mathbf{R}_i, \omega) = \sum_n \delta(\omega - E_n) |\langle i|\psi_n\rangle|^2, \tag{87}$$

where E_n and the $|\psi_n\rangle$ are the n-th eigenvalue and eigenvector, respectively. Physically, if an electron is initially placed at site $\mathbf{R}_i$, the local DOS at $\omega = E_F$ (Fermi energy) gives the amount of overlap of the local state at that

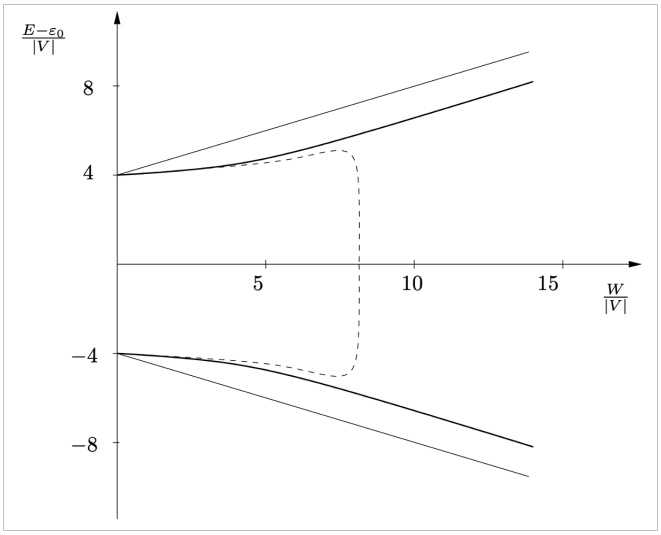

Figure 22. Localization for the Anderson model in the diamond lattice. The dashed line shows the mobility edges. The thin solid line shows the band edges and the thick solid line shows the edges of the band based on the Coherent Potential Approximation. Figure 9.1 of ref. [33].

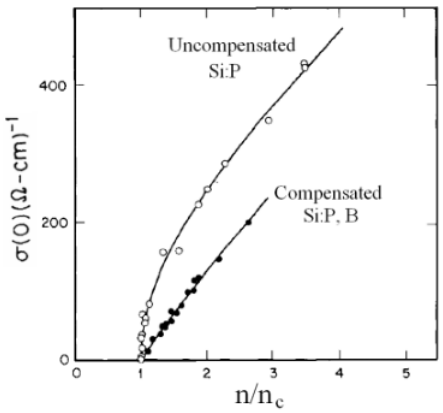

Figure 23. Zero-temperature conductivity of the semiconductor Si doped with P only (Si:P) or both P and B impurities (Si:P,B) as a function of impurity concentration. Figure taken from ref. [46].

site with other states at the same energy. The probability that the electron will propagate to other sites is then proportional to the local DOS, which can be viewed as a measure of the escape rate from that site. If it is zero, the particle will not diffuse to other sites. If it is finite, the particle will diffuse. However, as Anderson pointed out, this quantity is a random quantity and we must look at its *distribution*. It turns out that its distribution is extremely wide in the Anderson insulator. Fig. 24 shows the distributions of local DOS from a numerical solution of the Hamiltonian of Eq. (83). For a metallic phase, the local DOS shows a modestly broad, almost Gaussian distribution ($\gamma = 3t$ in the Figure; γ is the disorder strength, which we called W). On the other hand, in the localized phase ($\gamma = 18t$), the distribution is extremely broad and singular.

Because the distribution of local DOS in the insulator is so broad and singular, its average value is not a good measure of its *typical* value. What do we mean by typical value? There are a lot of different ways of defining a typical value. Examples are: the most probable value, the median of the distribution (i.e., the value such that there is a 50% chance that any other value is lower than it), or the geometric average

$$\rho_{typ}\left(\omega\right) = \exp\left(\overline{\ln\rho\left(\mathbf{R}_i,\omega\right)}\right). \tag{88}$$

The latter is the easiest to calculate numerically.

It turns out that, for a fixed energy, say, $\omega = 0$, as the disorder strength is increased, the average local DOS

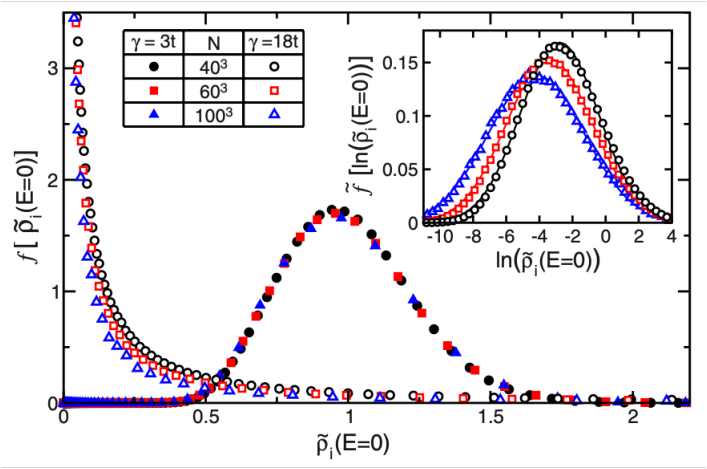

Figure 24. Distributions of the local density of states at the band center ($E = 0$) obtained from numerical diagonalization of the Hamiltonian of Eq. (83). Closed symbols correspond to extended states and open symbols to localized states. In this case, the critical value of disorder is $\gamma_c = W_c = 16.5t$. The inset shows the distribution of the logarithm of the local DOS for the localized phase. Figure taken from ref. [47].

$\overline{\rho(\omega = 0)}$ is finite and smooth as W crosses W_c, but the typical value, goes to zero at $W = W_c$

$$\rho_{typ}(\omega = 0) \sim (W_c - W)^{\beta}. \tag{89}$$

Thus, although the average local DOS is not a critical quantity and cannot be used to demarcate the transition, the typical value is the indicator of choice. It can be used as an order parameter for the Anderson metal-insulator transition.

VII. STATISTICAL DYNAMICAL MEAN-FIELD THEORY

The disordered DMFT approach, as already mentioned, does not capture the phenomenon of Anderson localization. If we want to establish a robust description of disordered strongly correlated systems, we must be able to incorporate Anderson localization effects. Fortunately, there is a natural extension of the disordered DMFT that does capture these effects. We call it natural because it retains the description of local correlation effects of DMFT while at the same time being able to fully describe Anderson localization. It has come to be named Statistical Dynamical Mean-Field Theory, or statDMFT [48].

In order to capture the basic physical idea behind statDMFT, we must first understand why DMFT fails to describe Anderson localization. We recall that in DMFT we must solve an *ensemble* of Anderson single-impurity problems [Eq. (5)] for a *fixed unique* hybridization function $\Delta(\omega)$ [Eq. (17)], thus generating the *ensemble* of local Green functions of Eq. (55) and corresponding local self-energies $\Sigma(\varepsilon_i, \omega)$. Physically, $\Delta(\omega)$ represents an average over all possible local hybridizations "seen" by the local sites. That there is an averaging process involved is perhaps best seen in Eq. (56), where the average local Green function $\overline{G_d(\omega)}$ is used in order to define the effective medium self-energy $\Sigma_{\rm EM}(\omega)$, which is later used to enforce self-consistency in Eq. (59). It is easy to show that, in the absence of interactions, the imaginary part of $\overline{G_d(\omega)}$ is precisely the local DOS of Eq. (87). So it is no surprise that no Anderson localization is possible in this approach: we have seen that the *average* local DOS is never critical and can never signal the Anderson localization transition.

So we now have an idea of what we must do: we must go beyond the average local Green function in the description. One possibility is to use the typical Green function, using, e.g., the geometric average. This has indeed been done [49, 50] and it gives interesting insight into the interplay between strong correlations and disorder. But yet another, even more ambitious approach is to use the *full distribution of local Green functions*. This is at the basis of the statDMFT approach.

We start by assuming that now each site sees a different hybridization function $\Delta(\mathbf{R}_i, \omega)$, not just an average value. We then solve each single-impurity problem for each site $\mathbf{R}_i$ of the lattice and obtain its local Green function

$$G_d(\mathbf{R}_i, \omega) = \frac{1}{\omega - \varepsilon_i - \Delta(\mathbf{R}_i, \omega) - \Sigma(\mathbf{R}_i, \omega)}. \tag{90}$$

The question now is how to implement self-consistency. We first note that, although the self-energy is site-dependent, it is local. A generic lattice Green function of a disordered interacting system, has a non-local self-energy

$$G_{\text{lat}}\left(\mathbf{R}_i, \mathbf{R}_j, \omega\right) = \frac{1}{\omega - H_0\left(\mathbf{R}_i, \mathbf{R}_j\right) - \Sigma\left(\mathbf{R}_i, \mathbf{R}_j, \omega\right)}, \tag{91}$$

where $H_0\left(\mathbf{R}_i, \mathbf{R}_j\right)$ is a site-basis representation of the non-interacting part of the Hamiltonian. The simplifying hypothesis of statDMFT is that we consider only local self-energies

$$\Sigma\left(\mathbf{R}_i, \mathbf{R}_j, \omega\right) \to \delta_{\mathbf{R}_i, \mathbf{R}_j} \Sigma\left(\mathbf{R}_i, \omega\right) \quad \text{(only in statDMFT)}, \tag{92}$$

so that

$$G_{\text{lat}}\left(\mathbf{R}_i, \mathbf{R}_j, \omega\right) = \frac{1}{\omega - H_0\left(\mathbf{R}_i, \mathbf{R}_j\right) - \delta_{\mathbf{R}_i, \mathbf{R}_j} \Sigma\left(\mathbf{R}_i, \omega\right)}. \tag{93}$$

We can now obtain the lattice Green function of Eq. (93) by doing a simple numerical matrix inversion of the right-hand side for a finite-sized system. Note that, since the self-energy is frequency-dependent, the matrix inversion has to be performed for each frequency. Once the inversion has been performed, the local part of the lattice Green function can be obtained (the matrix diagonal in the site-basis representation). We can then finally impose self-consistency with the initially determined local Green function of Eq. (90)

$$G_{\text{lat}}\left(\mathbf{R}_i, \mathbf{R}_i, \omega\right) = G_d\left(\mathbf{R}_i, \omega\right) = \frac{1}{\omega - \varepsilon_i - \Delta\left(\mathbf{R}_i, \omega\right) - \Sigma\left(\mathbf{R}_i, \omega\right)}. \tag{94}$$

The self-consistency loop is now the following:

1. Start with an initial guess for the set of hybridization functions $\Delta\left(\mathbf{R}_i, \omega\right)$, one for each site of a finite lattice.

2. Solve each impurity problem using some impurity solver to find $G_d\left(\mathbf{R}_i, t - t'\right) = -i\theta\left(t - t'\right) \left\langle \left\{ d_{\mathbf{R}_i,\sigma}\left(t\right), d^{\dagger}_{\mathbf{R}_i,\sigma}\left(t'\right) \right\} \right\rangle$.

3. Obtain its Fourier transform $G_d\left(\mathbf{R}_i, \omega\right)$.

4. Obtain the self-energy for each site from $\Sigma\left(\mathbf{R}_i, \omega\right) = \omega - \varepsilon_i - \Delta\left(\mathbf{R}_i, \omega\right) - \left[G_d\left(\mathbf{R}_i, \omega\right)\right]^{-1}$ [Eq. (90)].

5. Construct the frequency-dependent matrix

$$\omega - H_0\left(\mathbf{R}_i, \mathbf{R}_j\right) - \delta_{\mathbf{R}_i, \mathbf{R}_j} \Sigma\left(\mathbf{R}_i, \omega\right), \tag{95}$$

   invert it for each frequency and extract the diagonal elements $G_{\text{lat}}\left(\mathbf{R}_i, \mathbf{R}_i, \omega\right)$ [Eq. (93)].

6. Obtain a new set of hybridization functions from [Eq. (94)]

$$\Delta_{\text{new}}\left(\mathbf{R}_i, \omega\right) = \omega - \varepsilon_i - \Sigma\left(\mathbf{R}_i, \omega\right) - \left[G_{\text{lat}}\left(\mathbf{R}_i, \mathbf{R}_i, \omega\right)\right]^{-1}. \tag{96}$$

7. Test if $\Delta_{\text{new}}\left(\mathbf{R}_i, \omega\right) = \Delta\left(\mathbf{R}_i, \omega\right)$ for every site. If yes, self-consistency has been reached. If not, use $\Delta_{\text{new}}\left(\mathbf{R}_i, \omega\right)$ as the new set of hybridization functions and go back to step 1.

It is clear that this is a numerically very heavy task. Not only does one have to solve as many single-impurity problems as there are sites in the lattice, but also the self-consistency has to be achieved in *all of them*: there are also as many hybridization functions $\Delta\left(\mathbf{R}_i, \omega\right)$ as there are sites. Nevertheless, the procedure has been implemented for some problems

Let us also emphasize some important limits. If the disorder is turned off, statDMFT is equivalent to DMFT. In the limit of no interactions, the numerical procedure amounts to an exact diagonalization of the Anderson Hamiltonian and is, therefore, exact. When both disorder and interactions are present, statDMFT represents the most complete local approximation to the problem.

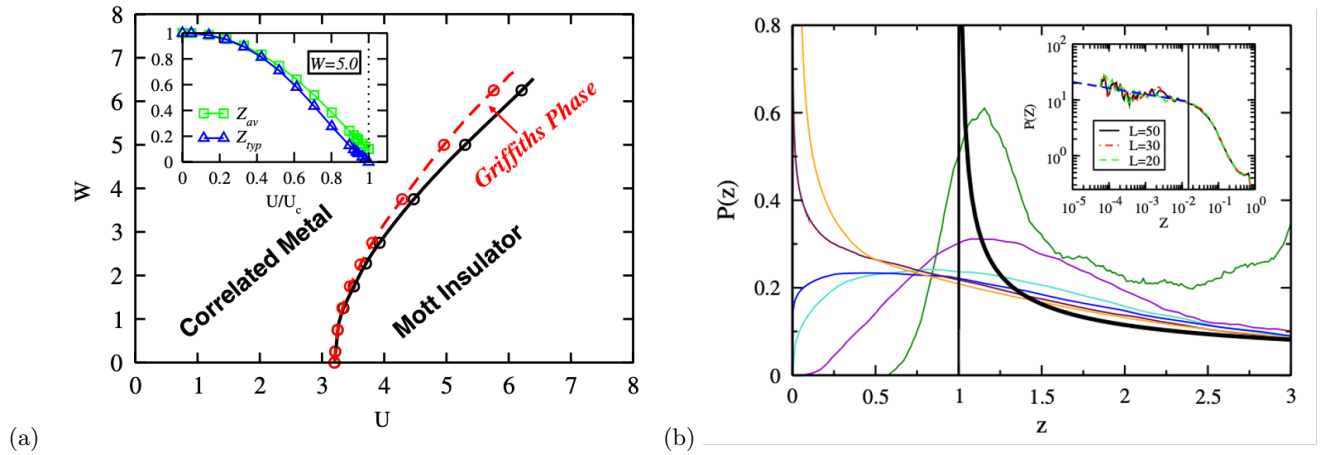

(a) (b)

Figure 25. (a) Zero-temperature, W/t (disorder) vs U/t (interaction) phase diagram of the two-dimensional disordered half-filled Hubbard model according to statDMFT. At the black line $U_c\left(W/t\right)$ all the quasi-particle weights Z_i vanish. The red line demarcates the Griffiths phase region. The inset shows the critical behavior of the average (Z_{av}) and the typical (Z_{typ}) quasi-particle weight; (b) Power-law distributions $P\left(z=Z/Z_0\right) \sim z^{\alpha-1}$ of quasi-particle weights for $U/U_c\left(W/t\right) = 0.6, 0.8, 0.9, 0.92, 0.94, 0.97$ for $W/t=5$. The thick black line is the DMFT distribution $P\left(Z^{\mathrm{DMFT}}\right)$ and Z_0 is the smallest quasi-particle weight in the DMFT treatment $Z_{\mathrm{min}}^{\mathrm{DMFT}}$. The inset shows the negligible dependence on lattice size for $U/U_c\left(W/t\right)=0.94$. Figure taken from ref. [51].

VIII. THE DISORDERED MOTT-HUBBARD TRANSITION ACCORDING TO STATDMFT

As a first application of statDMFT, let us look at the disordered Mott-Hubbard transition at $T=0$ of the two-dimensional half-filled Hubbard model with $L \times L$ sites, Eq. (53), which was considered in ref. [51]. A Fermi-liquid based impurity solver was used [52], which describes the local Green functions in a similar fashion to Eq. (62), but here generalized to the statDMFT scheme as

$$G_d\left(\mathbf{R}_i, \omega \approx 0\right) = \frac{1}{\omega - \varepsilon_i - \Delta\left(\mathbf{R}_i, \omega\right) - \Sigma\left(\mathbf{R}_i, \omega\right)} \approx \frac{Z_i}{\omega - Z_i\left[\varepsilon_i + \Delta'\left(\mathbf{R}_i, 0\right) + \delta_i\right] + iZ_i\left[\Delta''\left(\mathbf{R}_i, 0\right)\right]}. \tag{97}$$

Note that in this particular description the imaginary part of the local self-energy is zero, $\Gamma_i = 0$, meaning there are no inelastic scattering processes.

The quasi-particle weights show a distribution which we now analyze. We have seen that, within DMFT, all Z's vanish at the transition line $U_c\left(W\right)$, Eq. (63). Within statDMFT, however, the Mott transition is signaled by the vanishing of the *typical* quasi-particle weight Z_{typ}, here defined by the geometric average,

$$Z_{typ} = \exp\left(\overline{\ln Z}\right), \tag{98}$$

as $U \to U_c\left(W\right)$, meaning the destruction of most itinerant quasi-particles, which turn into local moments at a critical disorder-dependent interaction strength $U_c\left(W\right)$. The phase diagram thus obtained is shown in Fig. 25(a). The average value, Z_{av}, however, remains finite, meaning that very few sites remain empty or doubly occupied, see the inset of Fig. 25(a). Note that this is reminiscent of the behavior of the local DOS at the Anderson transition, see the discussion around Eq. (89).

Furthermore, the full distribution of Z_i's assumes a *universal* power-law shape with a non-universal power exponent α, see Fig. 25(b),

$$P\left(Z\right) \sim Z^{\alpha-1}. \tag{99}$$

Remembering that

$$T_{Ki} \sim Z_i, \tag{100}$$

this corresponds to a power-law distribution of local Kondo temperatures. The exponent α depends on both U and W and, when it falls below 1, the distribution becomes divergent as $Z_i \to 0$. The red line in Fig. 25(a) marks the point where $\alpha\left(U, W\right) = 1$.

There is a very simple way to understand why a power-law distribution emerges so universally (it is also seen in other models [53]). The following analysis was done in ref. [54]. First of all, it can be shown that the local Kondo temperature for a generic site described by Eq. (90) with $\varepsilon_i = 0$ (the effect of a non-zero ε_i does not change the results) can be written as

$$T_{Ki} = T_K^0 \exp\left(-x_i^2\right), \tag{101}$$

where T_K^0 is the Kondo temperature in the DMFT approximation and

$$x_i^2 = A\left\{\mathrm{Re}\left[\Delta\left(\mathbf{R}_i, \omega\right)\right]\right\}^2, \tag{102}$$

where the constant A can also be written in terms of quantities from the DMFT approximation. Therefore, the spatial fluctuations of the Kondo temperature are set by the fluctuations of the real part of the local hybridization functions. Now, disorder fluctuations lead, at weak and intermediate disorder (due to central limit theorem arguments), to Gaussian fluctuations of that real part, and hence of x_i, around a zero mean, so that

$$p\left(x_i\right) = \frac{1}{\sqrt{2\pi}\sigma_x} \exp\left[-\frac{x_i^2}{2\sigma_x^2}\right]. \tag{103}$$

In that case, it is easy to obtain the resulting T_K distribution

$$\begin{aligned} P\left(T_K\right) &= 2p\left[x\left(T_K\right)\right]\left|\frac{dx}{dT_K}\right| && (104)\\ &= \frac{2}{\sqrt{2\pi}\sigma_x} \exp\left\{-\frac{\left[x\left(T_K\right)\right]^2}{2\sigma_x^2}\right\} \frac{1}{2T_K\left|x\right|} && (105)\\ &= \frac{1}{\sqrt{2\pi}\sigma_x} \exp\left[\frac{\ln\left(T_K/T_K^0\right)}{2\sigma_x^2}\right] \frac{1}{T_K\left[\ln\left(T_K^0/T_K\right)\right]^{1/2}} && (106)\\ &= \frac{1}{\sqrt{2\pi}\sigma_x T_K^0\left[\ln\left(T_K^0/T_K\right)\right]^{1/2}} \left(\frac{T_K}{T_K^0}\right)^{\alpha-1}, && (107) \end{aligned}$$

where

$$\alpha = \frac{1}{2\sigma_x^2}. \tag{108}$$

Thus, up to very weak log-corrections, the distribution of Kondo temperatures is a power law, with a non-universal exponent that decreases as the disorder increases. The power-law form is an immediate consequence of disorder fluctuations of the band. It is also noteworthy that very mild disorder fluctuations lead to a singular distribution of Kondo temperatures, due to its exponential dependence.

The power-law above, together with the simple argument used to derive it, is a particular example of a more general phenomenon called quantum Griffiths phases [55]. These are characterized by the dominance of rare events in the determination of some physical quantity. Griffiths phases were first discussed in the context of classical magnetic systems [56], where they are disorder effects happening in the vicinity of magnetic phase transitions. In that context, however, they generally lead to extremely weak effects (essential singularities), that are very hard to detect. In quantum systems, on the other hand, their presence is felt by power laws and have a much better chance of being detected. Since the particular case we described above occurs not close to a magnetic phase transition but due to localization effects, it has been dubbed an *electronic Griffiths phase* [51, 53, 54].

Finally, there is disorder screening. We have seen this happen in DMFT, but it is also a feature of statDMFT. This is dramatically illustrated in Fig. 26, where we show the local DOS

$$\rho\left(\mathbf{R}_i, \omega\right) = -\frac{1}{\pi}\mathrm{Im}\left[G_d\left(\mathbf{R}_i, \omega\right)\right], \tag{109}$$

for each site of a 50×50 lattice with a color scale. Note how the fluctuations at the Fermi level $\omega = 0$ are very small (bottom figures) when compared to just slightly above it $\omega = 0.1 Z_{typ} D$ (top figures). *Both effects* are strongly enhanced as the transition is approached: (a) (a) $U/U_c = 0.87$ and (b) $U/U_c = 0.96$.

---

[1] J. Hubbard, Proc. Roy. Soc. (London) A **276**, 238 (1963).

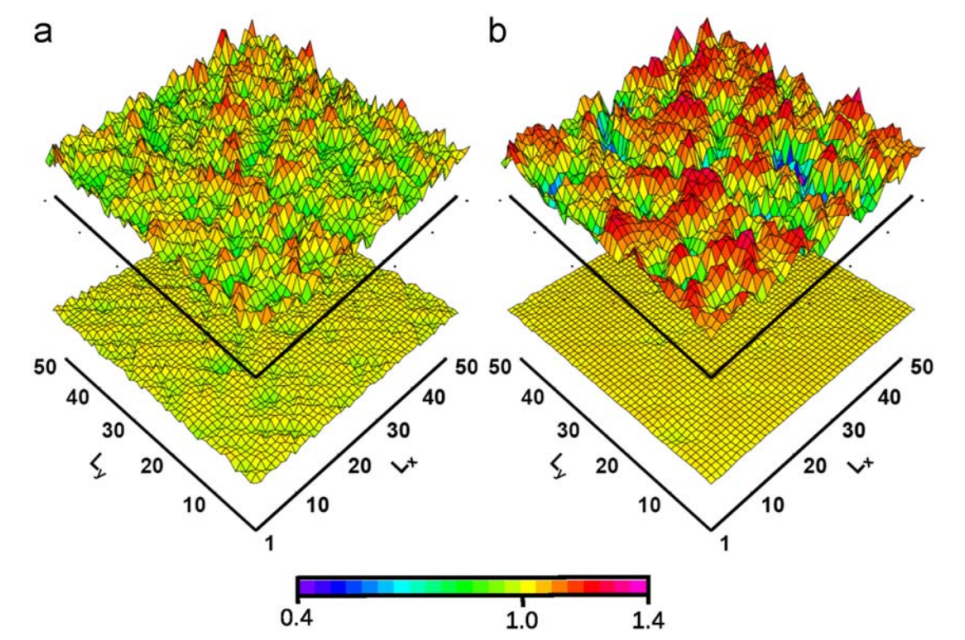

Figure 26. Spatial distribution of the local density of states of the two-dimensional disordered half-filled Hubbard model according to statDMFT, normalized by its clean and non-interacting value for one given realization of disorder and two distinct values of interactions: (a) $U/U_c = 0.87$ and (b) $U/U_c = 0.96$, where $U_c = 3.7D$, where D is the half band width. Top and bottom figures correspond to $\omega = 0.1 Z_{typ} D$ and $\omega = 0$, respectively. Figures taken from ref. [57].

[2] J. Hubbard, Proc. Roy. Soc. (London) A **277**, 237 (1964).
[3] J. Hubbard, Proc. Roy. Soc. (London) A **281**, 401 (1964).
[4] J. Hubbard, Proc. Roy. Soc. (London) A **285**, 542 (1965).
[5] P. W. Anderson, Phys. Rev. **79**, 350 (1950).
[6] P. W. Anderson, Phys. Rev. **124**, 41 (1961).
[7] P. Anderson and G. Yuval, Phys. Rev. Lett. **23**, 89 (1969).
[8] P. W. Anderson, J. Phys. C Solid State Phys. **3**, 2436 (1970).
[9] P. Anderson, G. Yuval, and D. Hamman, Phys. Rev. B **1**, 4464 (1970).
[10] K. G. Wilson, Rev. Mod. Phys. **47**, 773 (1975).
[11] N. Andrei, Phys. Rev. Lett. **45**, 379 (1980).
[12] P. B. Wiegmann, J. Phys. C Solid State Phys. **14**, 1463 (1981).
[13] N. Andrei, K. Furuya, and J. H. Lowenstein, Rev. Mod. Phys. **55**, 331 (1983).
[14] H. Krishna-murthy, J. Wilkins, and K. Wilson, Phys. Rev. B **21**, 1003 (1980).
[15] K. Yamada, Prog. Theor. Phys. **53**, 970 (1975).
[16] J. Allen, S. Oh, O. Gunnarsson, K. Schönhammer, M. Maple, M. Torikachvili, and I. Lindau, Adv. Phys. **35**, 275 (1986).
[17] M. Garnier, K. Breuer, D. Purdie, M. Hengsberger, Y. Baer, and B. Delley, Phys. Rev. Lett. **78**, 4127 (1997).
[18] L. D. Landau, Sov. Phys. JETP **3**, 920 (1957).
[19] L. D. Landau, Sov. Phys. JETP **5**, 101 (1957).
[20] L. D. Landau, Sov. Phys. JETP **8**, 70 (1959).
[21] P. Nozières, J. Low Temp. Phys. **17**, 31 (1974).
[22] A. C. Hewson, *The Kondo Problem to Heavy Fermions* (Cambrige University Press, Cambridge, 1993).
[23] A. Georges, G. Kotliar, W. Krauth, and M. J. Rozenberg, Rev. Mod. Phys. **68**, 13 (1996).
[24] G. Kotliar and D. Vollhardt, Phys. Today **57**, 53 (2004).
[25] W. Metzner and D. Vollhardt, Phys. Rev. Lett. **62**, 324 (1989).
[26] A. Georges and G. Kotliar, Phys. Rev. B **45**, 6479 (1992).
[27] M. Jarrell, Phys. Rev. Lett. **69**, 168 (1992).
[28] M. J. Rozenberg, X. Y. Zhang, and G. Kotliar, Phys. Rev. Lett. **69**, 1236 (1992).
[29] A. Georges and W. Krauth, Phys. Rev. Lett. **69**, 1240 (1992).
[30] S.-K. Mo, J. D. Denlinger, H.-D. Kim, J.-H. Park, J. W. Allen, A. Sekiyama, A. Yamasaki, K. Kadono, S. Suga, Y. Saitoh, T. Muro, P. Metcalf, G. Keller, K. Held, V. Eyert, V. I. Anisimov, and D. Vollhardt, Phys. Rev. Lett. **90**, 186403 (2003).
[31] H. Terletska, J. Vučičević, D. Tanasković, and V. Dobrosavljević, Phys. Rev. Lett. **107**, 026401 (2011).
[32] T. Furukawa, K. Miyagawa, H. Taniguchi, R. Kato, and K. Kanoda, Nat. Phys. **11**, 221 (2015).
[33] E. N. Economou, *Green's Functions in Quantum Physics* (Springer Berlin Heidelberg, 2006).

[34] D. Tanasković, V. Dobrosavljević, E. Abrahams, and G. Kotliar, Phys. Rev. Lett. **91**, 066603 (2003).
[35] M. C. O. Aguiar, V. Dobrosavljević, E. Abrahams, and G. Kotliar, Phys. Rev. B **71**, 205115 (2005).
[36] E. Miranda and V. Dobrosavljević, "Dynamical mean-field theories of correlation and disorder," in *Conductor-Insulator Quantum Phase Transitions*, edited by V. Dobrosavljević, N. Trivedi, and J. M. Valles (Oxford University Press, 2012) p. 161.
[37] E. Miranda, V. Dobrosavljević, and G. Kotliar, J. Phys.: Condens. Matter **8**, 9871 (1996).
[38] G. R. Stewart, Rev. Mod. Phys. **73**, 797 (2001).
[39] O. O. Bernal, D. E. MacLaughlin, H. G. Lukefahr, and B. Andraka, Phys. Rev. Lett. **75**, 2023 (1995).
[40] P. Coleman, *Introduction to Many-Body Physics* (Cambridge University Press, 2015).
[41] B. Andraka and G. R. Stewart, Phys. Rev. B **47**, 3208 (1993).
[42] E. C. Andrade, A. Jagannathan, E. Miranda, M. Vojta, and V. Dobrosavljević, Phys. Rev. Lett. **115**, 036403 (2015).
[43] K. Deguchi, S. Matsukawa, N. K. Sato, T. Hattori, K. Ishida, H. Takakura, and T. Ishimasa, Nat. Mater. **11**, 1013 (2012).
[44] P. W. Anderson, Phys. Rev. **109**, 1492 (1958).
[45] O. Schenk, M. Bollhöfer, and R. A. Römer, SIAM J. Sci. Comput. **28**, 963 (2006).
[46] M. A. Paalanen and R. N. Bhatt, Physica B **169**, 223 (1991).
[47] G. Schubert, J. Schleede, K. Byczuk, H. Fehske, and D. Vollhardt, Phys. Rev. B **81**, 155106 (2010).
[48] V. Dobrosavljević and G. Kotliar, Phil. Trans. R. Soc. Lond. A **356**, 1 (1998).
[49] V. Dobrosavljević, A. A. Pastor, and B. K. Nikolić, Europhys. Lett. **62**, 76 (2003).
[50] M. C. O. Aguiar, V. Dobrosavljević, E. Abrahams, and G. Kotliar, Phys. Rev. Lett. **102**, 156402 (2009).
[51] E. C. Andrade, E. Miranda, and V. Dobrosavljević, Phys. Rev. Lett. **102**, 206403 (2009).
[52] G. Kotliar and A. E. Ruckenstein, Phys. Rev. Lett. **57**, 1362 (1986).
[53] E. Miranda and V. Dobrosavljević, Phys. Rev. Lett. **86**, 264 (2001).
[54] D. Tanasković, E. Miranda, and V. Dobrosavljević, Phys. Rev. B **70**, 205108 (2004).
[55] T. Vojta, J. Low Temp. Phys. **161**, 299 (2010).
[56] R. B. Griffiths, Phys. Rev. Lett. **23**, 17 (1969).
[57] E. Andrade, E. Miranda, and V. Dobrosavljević, Physica B **404**, 3167 (2009).